T cells specific for α-myosin drive immunotherapy-related myocarditis

Axelrod, Margaret L.; Meijers, Wouter C.; Screever, Elles M.; Qin, Juan; Carroll, Mary Grace; Sun, Xiaopeng; Tannous, Elie; Zhang, Yueli; Sugiura, Ayaka; Taylor, Brandie C.

Published in:
Nature

DOI:
10.1038/s41586-022-05432-3

Publication date:
2022

Article

T cells specific for α-myosin drive immunotherapy-related myocarditis

https://doi.org/10.1038/s41586-022-05432-3

Received: 31 January 2022

Accepted: 7 October 2022

Published online: 16 November 2022

Check for updates

Margaret L. Axelrod[1], Wouter C. Meijers[1,2,3], Elles M. Screever[1,2,3], Juan Qin[1,4], Mary Grace Carroll[1], Xiaopeng Sun[1], Elie Tannous[1], Yueli Zhang[1], Ayaka Sugiura[1], Brandie C. Taylor[1], Ann Hanna[1], Shaoyi Zhang[4], Kaushik Amancherla[1], Warren Tai[1,5], Jordan J. Wright[1], Spencer C. Wei[6], Susan R. Opalenik[1], Abigail L. Toren[1], Jeffrey C. Rathmell[7,8,9], P. Brent Ferrell[1], Elizabeth J. Phillips[1,7,10,11,12], Simon Mallal[1,10,13], Douglas B. Johnson[1,8], James P. Allison[6,14], Javid J. Moslehi[1,4] ✉ & Justin M. Balko[1,7,8] ✉

Immune-related adverse events, particularly severe toxicities such as myocarditis, are major challenges to the utility of immune checkpoint inhibitors (ICIs) in anticancer therapy[1]. The pathogenesis of ICI-associated myocarditis (ICI-MC) is poorly understood. *Pdcd1*$^{-/-}$*Ctla4*$^{+/-}$ mice recapitulate clinicopathological features of ICI-MC, including myocardial T cell infiltration[2]. Here, using single-cell RNA and T cell receptor (TCR) sequencing of cardiac immune infiltrates from *Pdcd1*$^{-/-}$*Ctla4*$^{+/-}$ mice, we identify clonal effector CD8^{+} T cells as the dominant cell population. Treatment with anti-CD8-depleting, but not anti-CD4-depleting, antibodies improved the survival of *Pdcd1*$^{-/-}$*Ctla4*$^{+/-}$ mice. Adoptive transfer of immune cells from mice with myocarditis induced fatal myocarditis in recipients, which required CD8^{+} T cells. The cardiac-specific protein α-myosin, which is absent from the thymus[3,4], was identified as the cognate antigen source for three major histocompatibility complex class I-restricted TCRs derived from mice with fulminant myocarditis. Peripheral blood T cells from three patients with ICI-MC were expanded by α-myosin peptides. Moreover, these α-myosin-expanded T cells shared TCR clonotypes with diseased heart and skeletal muscle, which indicates that α-myosin may be a clinically important autoantigen in ICI-MC. These studies underscore the crucial role for cytotoxic CD8^{+} T cells, identify a candidate autoantigen in ICI-MC and yield new insights into the pathogenesis of ICI toxicity.

ICIs have substantially altered the treatment landscape and prognosis for many cancers. However, not all patients respond to treatment and many experience immune-related adverse events (irAEs), especially when ICIs are used in combination. Therefore, preventing, diagnosing and treating irAEs are urgent clinical challenges. Currently, clinically actionable biomarkers of response and toxicity are limited, and the mechanistic basis of irAEs is poorly defined.

Myocarditis is a rare irAE that affects <1% of patients receiving an ICI, but has a mortality rate of nearly 50%[1,5]. Combination ICI therapy (anti-PD-1 and anti-CTLA4 antibodies) is the most well-established risk factor for ICI-MC[6–9]. ICI-MC is pathologically characterized by the predominance of T cells and macrophages in the heart and often occurs together with myositis. Moreover, previous studies have demonstrated the presence of common clonotypes of cells in both tissue types[5]. These data indicate the possibility of shared target antigens that drive T cell expansion and activation, which would be crucial for pathogenesis; however, experimental data are lacking.

Generally, mice treated with ICIs do not replicate the full spectrum of irAEs seen in patients, which limits research into the mechanisms of toxicity. We recently described a mouse model of ICI-MC[2] in which C57BL6/J mice with homozygous knockout of *Pdcd1* and heterozygous deletion of *Ctla4* die prematurely and specifically due to myocarditis. Therefore, this mouse model recapitulates clinical and pathological features of ICI-MC[2]. Severe inflammation is specific to the heart in these mice. Flow cytometry analyses showed that the myocardial immune infiltrate is primarily composed of CD8^{+} T cells, similar to patients with ICI-MC. Furthermore, treatment with abatacept, a CTLA4 fusion protein, attenuates myocarditis and increases survival in the mice, consistent with previous clinical data from patients with ICI-MC treated with abatacept[2,10]. Here we use this mouse model of ICI-MC to

[1]Department of Medicine, Vanderbilt University Medical Center, Nashville, TN, USA. [2]Department of Cardiology, University Medical Center Groningen, Groningen, The Netherlands. [3]Department of Cardiology, Thorax Center, Erasmus University Medical Center, Rotterdam, Netherlands. [4]Section of Cardio-Oncology and Immunology, Division of Cardiology and the Cardiovascular Research Institute, University of California San Francisco, San Francisco, CA, USA. [5]Division of Cardiology, University of California, Los Angeles, CA, USA. [6]Department of Immunology, The University of Texas MD Anderson Cancer Center, Houston, TX, USA. [7]Department of Pathology, Microbiology and Immunology, Vanderbilt University Medical Center, Nashville, TN, USA. [8]Vanderbilt–Ingram Cancer Center, Vanderbilt University Medical Center, Nashville, TN, USA. [9]Vanderbilt Center for Immunobiology, Vanderbilt University Medical Center, Nashville, TN, USA. [10]Institute for Immunology and Infectious Diseases, Murdoch University, Perth, Australia. [11]Department of Dermatology, Vanderbilt University Medical Center, Nashville, TN, USA. [12]Department of Pharmacology, Vanderbilt University Medical Center, Nashville, TN, USA. [13]Department of Biomedical Informatics, Vanderbilt University Medical Center, Nashville, TN, USA. [14]Parker Institute for Cancer Immunotherapy, The University of Texas MD Anderson Cancer Center, Houston, TX, USA. ✉e-mail: Javid.Moslehi@ucsf.edu; justin.balko@vumc.org

characterize cardiac immune infiltrates. We establish CD8$^+$ T cells as necessary for disease and identify α-myosin as a cognate antigen for the most abundant TCRs in myocarditis. Furthermore, we extend these findings to human disease and show that α-myosin-expanded TCRs are present in inflamed cardiac and skeletal muscle in patients with ICI-MC.

Cardiac clonal CD8$^+$ T cells are abundant

Fulminant myocarditis affected 50% of *Pdcd1*$^{-/-}$*Ctla4*$^{+/-}$ mice and histological analyses showed destruction of the myocardial architecture[2] (Fig. 1a,b). Incidence was higher in female mice, which is in line with data in patients that female sex is a risk factor for developing ICI-MC[2,9]. The myocardial immune infiltrate in affected mice was primarily composed of CD8$^+$ T cells and did not differ by sex[2] (Extended Data Fig. 1a). No significant antibody deposits or B220$^+$ B cells were observed in the hearts of mice with myocarditis, which provided support for the further study of T cells at the site of disease (Extended Data Fig. 1b). We used single-cell RNA and TCR sequencing (scRNA–TCR-seq) to characterize sorted CD45$^+$-infiltrating immune cells from the hearts of four *Pdcd1*$^{-/-}$*Ctla4*$^{+/-}$ mice affected by myocarditis and six healthy wild-type mice. Dimensionality reduction with uniform manifold approximation and projection (UMAP), clustering with Louvain and cluster cell-type annotation assisted by SingleR showed distinct immune cell populations in myocarditis compared with control samples (Fig. 1c and Extended Data Fig. 2a). The largest difference was seen in the activated T cell cluster, which made up 34% of the myocarditis immune cells and only 2% of the control immune cells. Markers of activation such as *Ccl5*, *Ccl4*, *Tigit*, *Nkg7* and *Gzmb* were upregulated in the T cell clusters in myocarditis compared with control T cell clusters (Extended Data Fig. 2b). Conversely, markers of naive status such as *Ccr7*, *Lef1* and *Sell* were upregulated in control T cells. Activation markers were also upregulated in other clusters, including myeloid cell subsets, in the myocarditis samples (Extended Data Fig. 2c). *AW112010*, a long noncoding RNA essential for the orchestration of mucosal immunity during infections and in colitis, was strongly upregulated in several clusters in the myocarditis samples[11,12]. By contrast, B cells made up most of the immune cells in the control samples, which is consistent with previous studies[13–15].

To further characterize T cells, we performed dimensionality reduction and clustering on *Cd3e*$^+$ and TCR$^+$ cells, which showed differential cluster abundance in myocarditis compared with control samples (Fig. 1d). Differential gene expression analyses and plotting of key identity genes revealed distinct cluster identities (Fig. 1e and Extended Data Fig. 3a). Cluster 0 cells were activated effector CD8$^+$ T cells that expressed *Gzmb*, *Ifng* and *Nkg7*. Cluster 1 cells were resting CD8$^+$ T cells that expressed *Ccr7*, *Sell* and *Klf2*. Cluster 2 cells were CD4$^+$ T cells that expressed *Cd4*, *Ccr7* and *Cd40lg*. Cluster 3 cells were proliferative CD8$^+$ T cells that expressed *Mki67*, *Cdk1* and *Tk1*. Cluster 4 cells were *Cd24a*-expressing T cells and constituted a small fraction of the total T cells. CD24 is upregulated with TCR signalling and is necessary for T cell proliferative capacity[16,17]. Cluster 0 (effector CD8$^+$T cells) constituted most of the myocarditis cells. Cluster 3 (proliferating CD8$^+$ T cells) and cluster 0 were enriched in the myocarditis sample relative to the control sample. Cluster 0 and cluster 3 also had the highest TCR density, defined as the number of neighbouring cells with the same TCR α chain and β chain. High TCR density was limited to the myocarditis sample (Fig. 1f). Genes upregulated in cluster 0 T cells included *Ccl5*, *Nkg7*, *Ccl4*, *Cxcr6*, *Lag3* and *Prf1* (Fig. 1g and Extended Data Fig. 3b). We also sought to investigate genes associated with tissue residency, as intravascular immune cells were not excluded in our tissue preparation protocol. We found substantial expression of *Cd69*, *Itgb1*, *Itgal*, *Cxcr3*, *Cxcr6* and *Runx3* in myocarditis T cell clusters, whereas levels of these genes were lower in control T cells[18,19] (Extended Data Fig. 3c). These data suggest that myocarditis T cells are CD8$^+$, tissue-resident, effector and proliferating.

We next sought to assess the clonality of TCRs in the myocarditis samples using both bulk and single-cell TCR-seq. Cardiac tissue from affected *Pdcd1*$^{-/-}$*Ctla4*$^{+/-}$ mice had lower Shannon diversity than splenic tissue from healthy wild-type mice or mice with myocarditis. This result indicated a higher degree of clonal TCRs in mycocarditis (Extended Data Fig. 3d), which did not differ by sex. No clonal (>2 cells with the same TCR clonotype) cells were identified by single-cell TCR-seq of cardiac immune infiltrate from healthy mice. By contrast, 63% of TCR$^+$ cells in the myocarditis samples represented clonal TCRs (Extended Data Fig. 3e). A comparison of gene expression by clonality showed that non-clonal cells from control samples expressed *Cd8a*, *Cd4* and markers associated with naive status rather than activation. By contrast, clonal cells from myocarditis samples expressed *Cd8a* and cytotoxicity genes such as *Nkg7* and *Gzmb*, but not *Cd4* or markers of naive status (Fig. 1h). These data show that there is a large population of highly activated, clonally expanded CD8$^+$ T cells in mouse ICI-MC.

CD8$^+$ T cells are necessary for myocarditis

Early administration of corticosteroids, which exert immunosuppressive effects through various mechanisms, may associate with better survival in patients with ICI-MC, but severe cases are refractory to steroids[20,21]. In our mouse model, dexamethasone treatment did not attenuate myocarditis or extend survival, which provides support for the severity of the phenotype (Extended Data Fig. 4a). Using anti-CD8-depleting and anti-CD4 depleting antibodies (starting at 21 days of age and administered three times per week; confirmation shown in Extended Data Fig. 4b), we tested whether depletion of these cell subsets would attenuate myocarditis and affect survival of *Pdcd1*$^{-/-}$*Ctla4*$^{+/-}$ mice. Depletion of CD8$^+$ cells but not CD4$^+$ cells significantly rescued survival in these mice (Fig. 2a). In corroboration of these data, adoptive transfer of whole splenocytes, but not splenocytes from which CD8$^+$ cells were depleted (Extended Data Fig. 4c), from *Pdcd1*$^{-/-}$*Ctla4*$^{+/-}$ mice with myocarditis to *Rag1*$^{-/-}$ recipients was sufficient to induce fatal myocarditis (Fig. 2b,c). The single fatality in the CD8-depleted group was probably due to a bowel obstruction, as there was no evidence of myocarditis histologically. Immunohistochemistry (IHC) showed abundant cardiac infiltration of CD3$^+$ and CD8$^+$ cells, and limited CD4$^+$ cells and F4/80$^+$ cells, in the recipients of whole splenocytes but not in the CD8-depleted recipients (Fig. 2d and Extended Data Fig. 4d). We performed TCR β chain sequencing of cardiac tissue from one donor mouse (donor) and from four recipients of whole splenocytes (Rec1–Rec4) (Fig. 2e). High numbers (>2,000) of TCR reads were seen in all sequenced hearts, which indicated the presence of significant T cell infiltration, consistent with the histology results (Extended Data Fig. 4e). In all four of the recipient mice, the most clonal TCR β chain occupied >65% of the total cardiac TCR repertoire, which indicated that there was strong monoclonal expansion. The most clonal TCR β chain (CDR3: CASSLRRGEQYF) in the donor heart (which constituted 37% of the donor cardiac repertoire) was expanded in three out of the four recipients (Rec1, Rec3 and Rec4). Notably, in one recipient mouse (Rec2), a low frequency TCR from the donor was expanded and occupied most of the TCR β chain repertoire (CDR3: CASSLGGTVQDTQYF). This high degree of expansion from donor to recipient cardiac tissue suggests that a single TCR clonotype may drive myocarditis in the recipient animals. Together, these results strongly indicate that CD8$^+$ T cells are necessary for the development of myocarditis.

Myocarditis TCRs recognize α-myosin

Next we aimed to identify the cognate antigen for clonal mouse TCRs. For antigen discovery, we tested five TCRs derived from scRNA–TCR-seq data and selected on the basis of their abundance. These TCRs (TCR-A and TCR1–TCR4) were primarily associated with cluster 0 effector CD8$^+$ T cells and cluster 3 proliferating T cells (Fig. 3a). We also included two

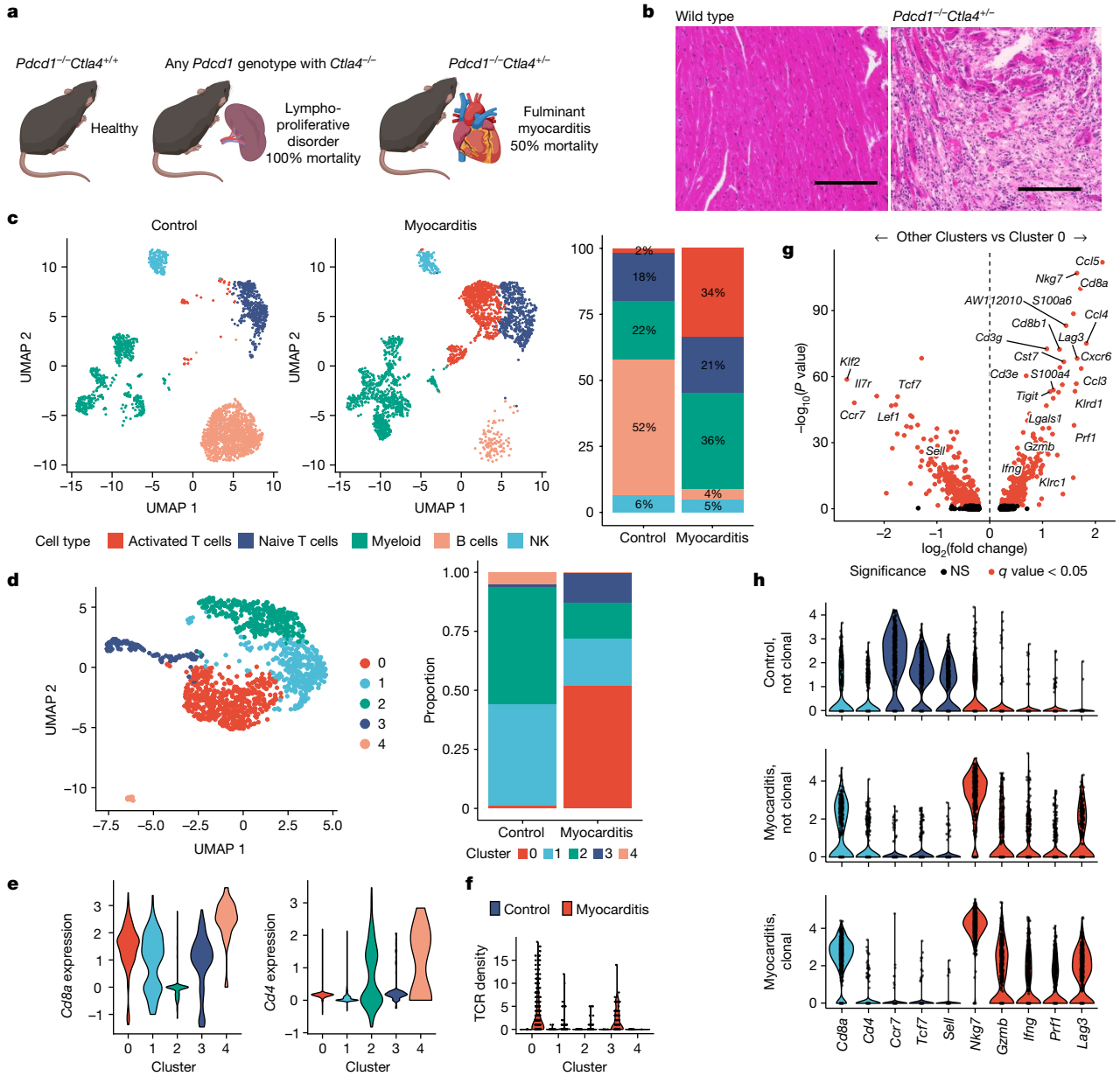

Fig. 1 | scRNA–TCR-seq reveals abundant clonal effector CD8⁺ T cells in ICI-MC. a, Phenotypic summary of mice with *Pdcd1* and *Ctla4* genetic loss. *Pdcd1*$^{-/-}$*Ctla4*$^{+/+}$ mice do not have an overt phenotype. Mice with complete loss of *Ctla4* have a fatal lymphoproliferative disorder regardless of *Pdcd1* genotype. *Pdcd1*$^{-/-}$*Ctla4*$^{+/-}$ mice develop fulminant myocarditis. **b**, Cardiac tissue from a healthy wild-type mouse and a *Pdcd1*$^{-/-}$*Ctla4*$^{+/-}$ mouse with myocarditis stained with haematoxylin and eosin (H&E). Images representative of $n = 10$ mice per genotype. Scale bar, 200 µm. **c**, Dimensionality reduction with UMAP of scRNA-seq data of sorted CD45⁺ immune cells from hearts of control wild-type mouse ($n = 6$) and *Pdcd1*$^{-/-}$*Ctla4*$^{+/-}$ mice with myocarditis ($n = 4$) ($n = 2{,}509$ cells per genotype). Cell-type annotations were assisted by SingleR and are quantified on the right. NK, natural killer. **d**, UMAP was subset on cells with *Cd3e* expression levels >1.5 and the presence of a TCR, and then clustered using the Louvain algorithm ($n = 1{,}266$ cells). The proportion of T cells from control samples and myocarditis samples in each cluster is quantified on the right. **e**, Expression of the key T cell identity genes *Cd8a* and *Cd4* are shown for each T cell cluster. **f**, TCR density is a measure of how many of the 100 nearest neighbours share the same TCR α chain and β chain. TCR density is shown for each cluster and split by control or myocarditis. **g**, Differential gene expression between cluster 0 T cells and all other T cell clusters (1, 2, 3 and 4). Higher expression in cluster 0 is indicated by positive fold-change. Red indicates false-discovery-rate-corrected *P* value (*q* value) < 0.05. Black indicates non-significance (NS). **h**, Violin plots of expression of key genes by clonality and sample. Clonal is defined as >2 cells with the same TCR α chain and β chain. No clonal cells are seen in the control sample. Identity genes are in light blue. Naive T cells genes are in dark blue. T cell activation genes are red. Panel **a** was created with BioRender.com.

TCRs that were expanded the hearts of recipient mice in adoptive transfer experiments (TCR-B and TCR-C). TCR-B was the most abundant TCR in the heart of the donor and three recipients (β CDR3: CASSLRRGEQYF). TCR-C was the most abundant TCR in the heart of recipient 2 (β CDR3: CASSLGGTVQDTQYF) (Fig. 2e). CDR3 amino acid sequences, V genes and J genes are shown in Table 1. These TCRs were reconstructed using Stitchr, cloned and retrovirally transduced into Jurkat nuclear factor of activated T cells (NFAT) cells expressing GFP as the reporter[22–24]. Syngeneic bone-marrow-derived dendritic cells (BMDCs) were used as antigen-presenting cells (APCs).

We used a candidate autoantigen approach for TCR screening. Analysis of published human RNA-seq data of thymic APCs showed four

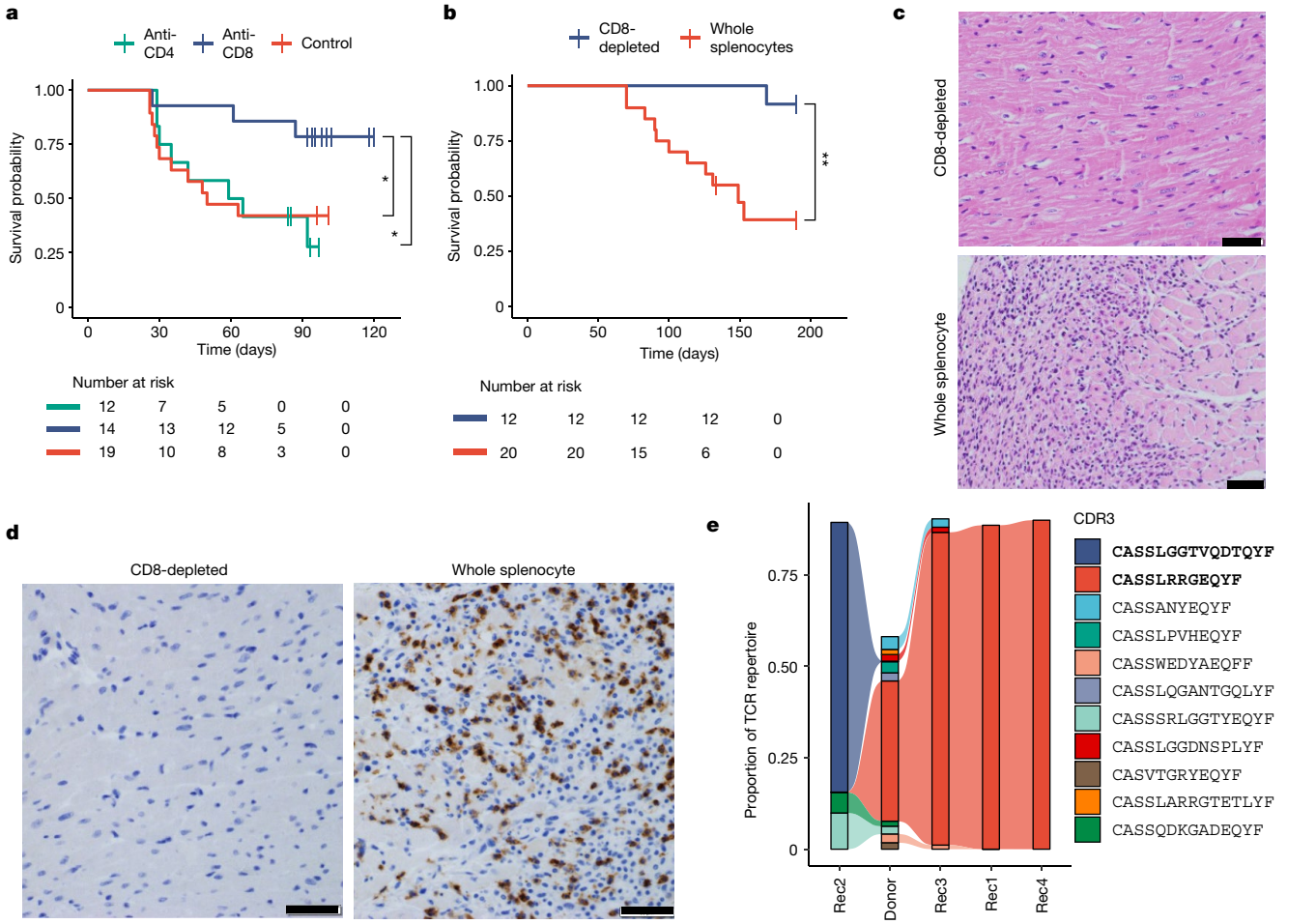

Fig. 2 | CD8$^+$ T cells are necessary for myocarditis. a, *Pdcd1*$^{-/-}$ *Ctla4*$^{+/-}$ mice were treated with anti-CD4-depleting, anti-CD8-depleting, or control antibodies. Antibody treatments were started at 21 days of age and administered three times per week. Time was measured since birth, but no mice were censored before the start of the experiment at day 21. $P = 0.03$, anti-CD8 versus control, $P = 0.02$, anti-CD8 versus anti-CD4, two-sided Cox proportional hazard tests. Risk table below shows the size of groups. **b**, Whole splenocytes or splenocytes from which CD8 cells were depleted from *Pdcd1*$^{-/-}$ *Ctla4*$^{+/-}$ mice with myocarditis were transferred to *Rag1*$^{-/-}$ recipient mice. Day 0 is the day of adoptive transfer. $P = 0.0017$, two-sided Cox proportional hazard test. Risk table below shows the size of groups. **c**, Representative H&E-stained images from CD8-depleted splenocyte recipients compared with whole-splenocyte recipients. Only cardiac sections are shown. Representative of $n = 10$ mice per group. Scale bars, 50 µm. **d**, Representative IHC for CD8 on cardiac sections from CD8-depleted splenocyte recipients compared with whole-splenocyte recipients. Scale bars, 50 µm. Representative of $n = 10$ mice per group. **e**, TCR β chain sequencing of cardiac tissue from a donor *Pdcd1*$^{-/-}$ *Ctla4*$^{+/-}$ mouse (donor) and *Rag1*$^{-/-}$ whole-splenocyte recipients (Rec1–Rec4). The top ten most abundant TCRs from the donor plus the most abundant TCR from Rec2 are shown. Flow between samples indicates shared TCRs. CDR3 sequences in bold indicate the most clonal TCRs.

cardiac-enriched genes (genes in which expression in the heart was significantly enriched relative to other tissues) with no detectable expression in the thymus[4] (*MYH6*, *NPPA*, *NPPB* and *SBK2*) (Fig. 3b). Lack of thymic expression would be predicted to enable self-reactive T cells to escape negative selection, an important mechanism of self-tolerance. Expression of these genes was also low to absent in the thymus of *Pdcd1*$^{-/-}$ *Ctla4*$^{+/-}$ mice and did not differ by sex (Extended Data Fig. 5a). We used a library of 172 overlapping peptides, covering all of α-myosin (encoded by *Myh6*), ANP (encoded by *Nppa*), BNP (encoded by *Nppb*) and SBK2 (encoded by *Sbk2*) (Extended Data Table 1). Three TCR cell lines, including both expanded TCRs (B and C), had NFAT activity in response to α-myosin peptides. None of the other three tested cardiac proteins activated any of the TCR cell lines (Fig. 3c). *MYH6* (α-myosin) is not expressed in the thymus in mice or humans and is a major histocompatibility class II (MHC-II)-restricted autoantigen in mouse models[3,25,26]. Notable, four out of five single-cell-derived TCR cell lines did not recognize any of the tested cardiac peptides (denoted TCR1–TCR4 to differentiate from TCR-A to TCR-C from which cognate antigens were identified). These data suggest two important possibilities: (1) the presence of 'bystander' T cells that are attracted to the site of inflammation but are not specific for disease-causing antigens or (2) the possibility that these TCRs recognize other cardiac antigens that are important in disease pathogenesis. The bystander TCR hypothesis is supported by previous literature on tumour immunology showing that a minority of tumour-infiltrating T cells are likely to be tumour-specific[27–31].

TCR-A and TCR-B activated NFAT reporters in response to the same α-myosin peptide ($MYH6_{181–200}$), whereas TCR-C had NFAT activity against a distinct α-myosin peptide ($MYH6_{406–425}$) (Fig. 3c). From these 20-amino-acid peptides, we used TepiTool to identify the most probable immunogenic epitopes[32] and re-screened these epitopes against the reporter TCR lines. TCR-A and TCR-B recognized $MYH6_{191–198}$ (VIQYFASI), whereas TCR-C recognized $MYH6_{418–425}$ (VQQVYYSI) (Fig. 3d). VIQYFASI and VQQVYYSI both had strong predicted binding to H2-Kb (Extended Data Table 2). The tyrosine and phenylalanine residues at position five of the peptides are key binding epitopes for H2-Kb[33]. In line with these predictions, antibody blockade of H2-Kb, but not H2-Db, abrogated

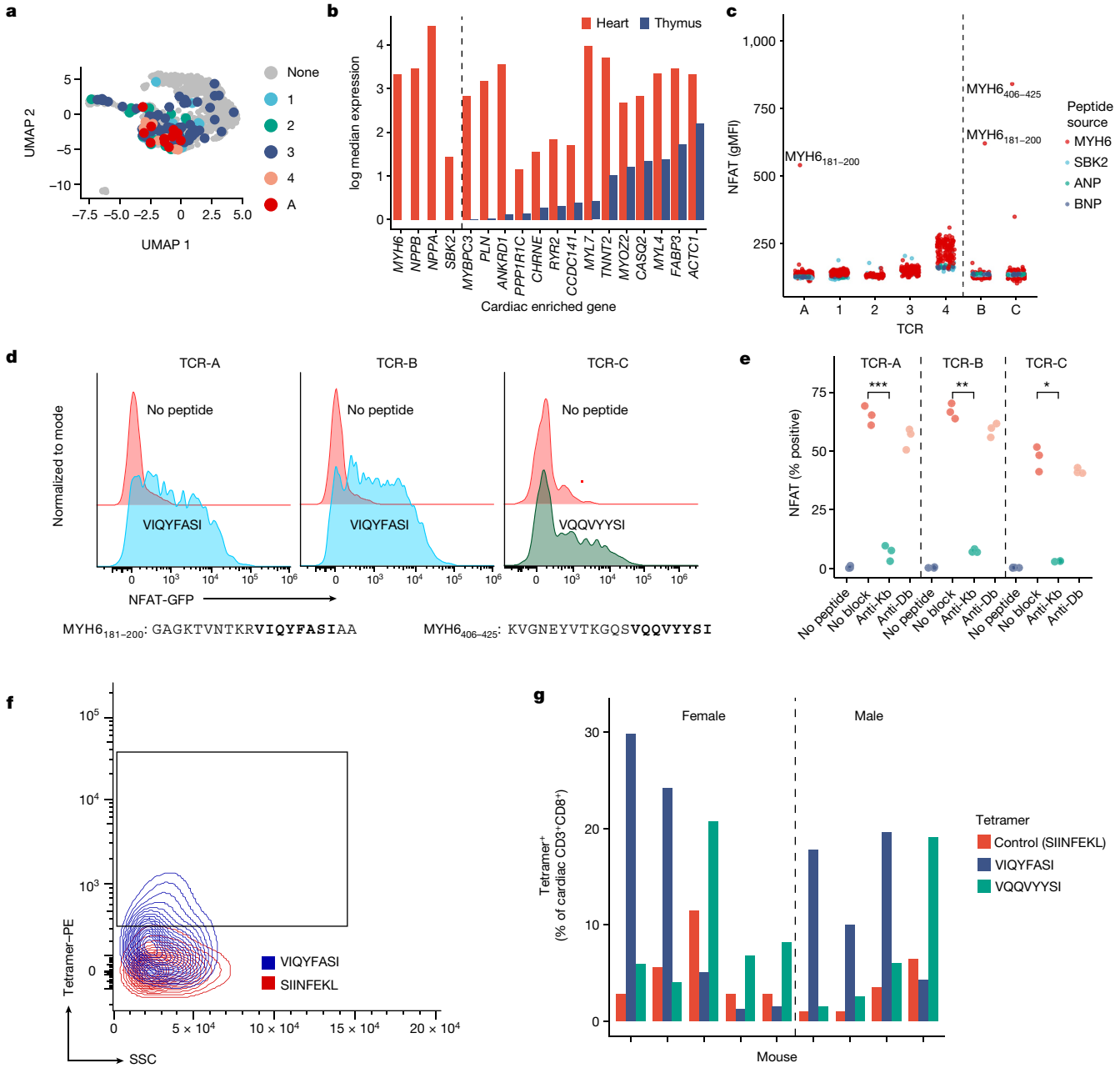

Fig. 3 | α-myosin is a MHC-I-restricted autoantigen in mouse myocarditis. **a**, TCR-A and TCR1–TCR4, used for antigen discovery, are shown on the same plot as Fig. 1d. Grey cells do not express TCR-A or TCR1–TCR4. **b**, The log-transformed median expression of 18 cardiac-enriched genes in the heart and thymus. Genes to the left of the dashed line have no detectable expression in thymic APCs. **c**, NFAT–GFP reporter activity, measured by flow cytometry and shown as geometric mean fluorescence intensity (gMFI), of all TCR cell lines stimulated independently with 172, 10–20 amino-acid-long SBK2, ANP, BNP or α-myosin peptides. TCRs to the left of the dotted line are derived from single-cell sequencing data (**a**). TCRs to the right of the dotted line were selected due to expansion in adoptive transfer experiments (Fig. 2e). TCRs named with letters (A–C) have a cognate antigen identified, whereas TCRs named with numerals (1–4) do not have an identified cognate antigen. Top α-myosin peptide hits are labelled. **d**, Representative ($n = 3$ independent replicates) flow cytometry histograms of each TCR cell line co-cultured with BMDCs and stimulated with 10 μg ml^{-1} predicted cognate peptide relative to no peptide. Peptide sequences are shown below the plots. **e**, Each TCR cell line was co-cultured with EL-4 APCs and 10 μg ml^{-1} cognate peptide (VIQYFASI for TCR-A and TCR-B; VQQVYYSI for TCR-C; except for no peptide controls) with or without 10 μg ml^{-1} of anti-Kb or anti-Db blocking antibody. NFAT–GFP reporter activity is shown as the percentage of live cells. $n = 3$ biological replicates. $P = 0.00035$ (TCR-A), $P = 0.004$ (TCR-B), $P = 0.013$ (TCR-C), two-sided t-tests for no block to anti-Kb, adjusted for multiple comparisons. **f**, Representative flow cytometry of SIINFEKL-loaded or VIQYFASI-loaded H2-Kb tetramer staining on cardiac CD3$^+$CD8$^+$ cells. **g**, Quantification of control, VIQYFASI and VQQVYYSI H2-Kb tetramer staining in cardiac CD3$^+$CD8$^+$ cells in individual mice. Each group of three bars represents one mouse with myocarditis. $n = 5$ female and 4 male mice.

NFAT reporter activity for all three cell lines (Fig. 3e). Next we compared an empty H2-Kb tetramer loaded with either VIQYFASI or VQQVYYSI with a tetramer loaded with an irrelevant peptide (SIINFEKL). We found that 6–30% of the cardiac-infiltrating CD8$^+$ T cells were specific for one of the two α-myosin peptides in nine additional *Pdcd1*$^{-/-}$*Ctla4*$^{+/-}$ mice with myocarditis (Fig. 3f,g and Extended Data Fig. 5b). We did not identify any mice with myocarditis that lacked VIQYFASI or VQQVYYSI tetramer-positive CD8$^+$ T cells in their hearts. This result demonstrates

Table 1 | Summary of TCR CDR3, V and J genes for TCRs used in antigen discovery experiments

TCR ID	TCR source	βCDR3	TRBV	TRBJ	αCDR3	TRAV	TRAJ	Antigen
A	Mouse single-cell sequencing	CSAAWGGSAETLYF	TRBV1	TRBJ2-3	CAVSDRGSALGRLHF	TRAV7-3*04	TRAJ18	$MYH6_{191–198}$ (VIQYFASI)
1	Mouse single-cell sequencing	CASSPGQGAYAEQFF	TRBV12-2	TRBJ2-1	CAVSSGYGSSGNKLIF	TRAV7-5	TRAJ32	Unknown (not in α-myosin, SBK2, ANP or BNP)
2	Mouse single-cell sequencing	CASKTGYNYAEQFF	TRBV19	TRBJ2-1	CALNTGYQNFYF	TRAV4-4-DV10	TRAJ49	Unknown (not in α-myosin, SBK2, ANP or BNP)
3	Mouse single-cell sequencing	CASGGLGGPSQNTLYF	TRBV12-2	TRBJ2-4	CALERSTGNYKYVF	TRAV13-1	TRAJ40	Unknown (not in α-myosin, SBK2, ANP or BNP)
4	Mouse single-cell sequencing	CASSDAGYAEQFF	TRBV13-3	TRBJ2-1	CALGDSNYQLIW	TRAV6-6	TRAJ33	Unknown (not in α-myosin, SBK2, ANP or BNP)
B	Adoptive transfer (donor, Rec1, Rec3 or Rec4)	CASSLRRGEQYF	TRBV15	TRBJ2-7	CALERASGSWQLIF	TRAV13-1	TRAJ22	$MYH6_{191–198}$ (VIQYFASI)
C	Adoptive transfer (Rec2)	CASSLGGTVQDTQYF	TRBV12-2	TRBJ2-5	CALGDRNNAGAKLTF	TRAV6D-6	TRAJ39	$MYH6_{418–425}$ (VQQVYYSI)
TCR-Pt1	Patient 1 exPBMCs (single-cell sequencing)	CASSPYQSSGANVLTF	TRBV9	TRBJ2-6	CALSDRYGGATNKLIF	TRAV19	TRAJ32	$MYH6_{443–451}$ (RINATLETK)

the ubiquity of α-myosin-reactive T cells in this mouse model. Notably, high levels of α-myosin tetramer-positive $CD8^+$ T cells were confined to the hearts (Extended Data Fig. 5c). These data strongly suggest that α-myosin is an important MHC-I-restricted autoantigen in mouse immune checkpoint deficiency myocarditis.

α-myosin TCRs are found in patients with ICI-MC

We next aimed to test the relevance of α-myosin as a potential autoantigen in humans. We analysed samples from three healthy donors and from three patients with histologically proven fulminant ICI-MC. Patient information is summarized in Table 2. First, we tested whether it was possible to expand α-myosin-specific T cells from peripheral blood mononuclear cells (PBMCs). PBMCs were stimulated with α-myosin peptides or with control cytomegalovirus, Epstein–Barr virus and influenza (CEF) peptides (in healthy donor PBMCs only) for 14 days to generate expanded PBMCs (exPBMCs). TCR β chain sequencing was used to assess expansion. Shannon diversity decreased from pre-expansion PBMCs to α-myosin exPBMCs for healthy donors and for patients with ICI-MC, which indicated the presence of clonal expansion of α-myosin-specific T cells. Notably, Shannon diversity did not change from baseline to CEF peptide expansion, which suggested that α-myosin is a strong stimulus for clonal T cell expansion (Fig. 4a). For all donors, both α-myosin and CEF stimulation resulted in the expansion of some individual TCR clonotypes. This expansion could be seen by comparing the frequency of each TCR β chain in the baseline PBMCs compared with the exPBMCs from the same patient (Extended Data Fig. 6a,b). These data suggest that both healthy donors and patients with ICI-MC have peripheral α-myosin-specific T cells that are capable of expansion under certain conditions.

Table 2 | Summary of information for patients with myocarditis

Patient	Age (years)	Sex	ICI history	Primary tumour	Disease tissue TCR-seq	Brief clinical course
1	75	Male	Ipilimumab and nivolumab	Renal cell carcinoma	Cardiac biopsy; autopsy of diaphragm and psoas	The patient presented to the emergency department with chest pain 3 weeks after initiation of ICI and was found to have VT and elevated troponin. EMB confirmed myocarditis. The patient's clinical course was complicated by cardiogenic shock, acute hypoxic respiratory failure and acute renal failure, despite high-dose steroids. The patient and family declined further aggressive treatment with curative intent and opted for palliative extubation.
2	64	Male	Nivolumab	Small cell lung cancer	Autopsy of RV and LV, interventricular septum, deltoid and diaphragm	The patient was admitted to the hospital with recurrent VT and elevated troponin. The patient was found to have a dilated RV by echocardiography. Prednisone treatment was initiated. EMB was complicated by RV perforation leading to acute cardiac tamponade, left atrial thrombus and rapid clinical deterioration. Family opted for palliative extubation.
3	78	Male	Pembrolizumab	Lung adenocarcinoma	Cardiac biopsy	The patient was evaluated for fatigue and myalgias and was found to have elevated troponin. The patient was admitted, started on high-dose steroids and myocarditis was confirmed by EMB. The patient recovered with steroid treatment and did not experience recurrence of myocarditis. The patient died 5 months later in home hospice owing to complications related to a haemothorax, which was potentially related to the underlying malignancy.

EMB, endomyocardial biopsy; LV, left ventricle; RV, right ventricle; VT, ventricular tachycardia.

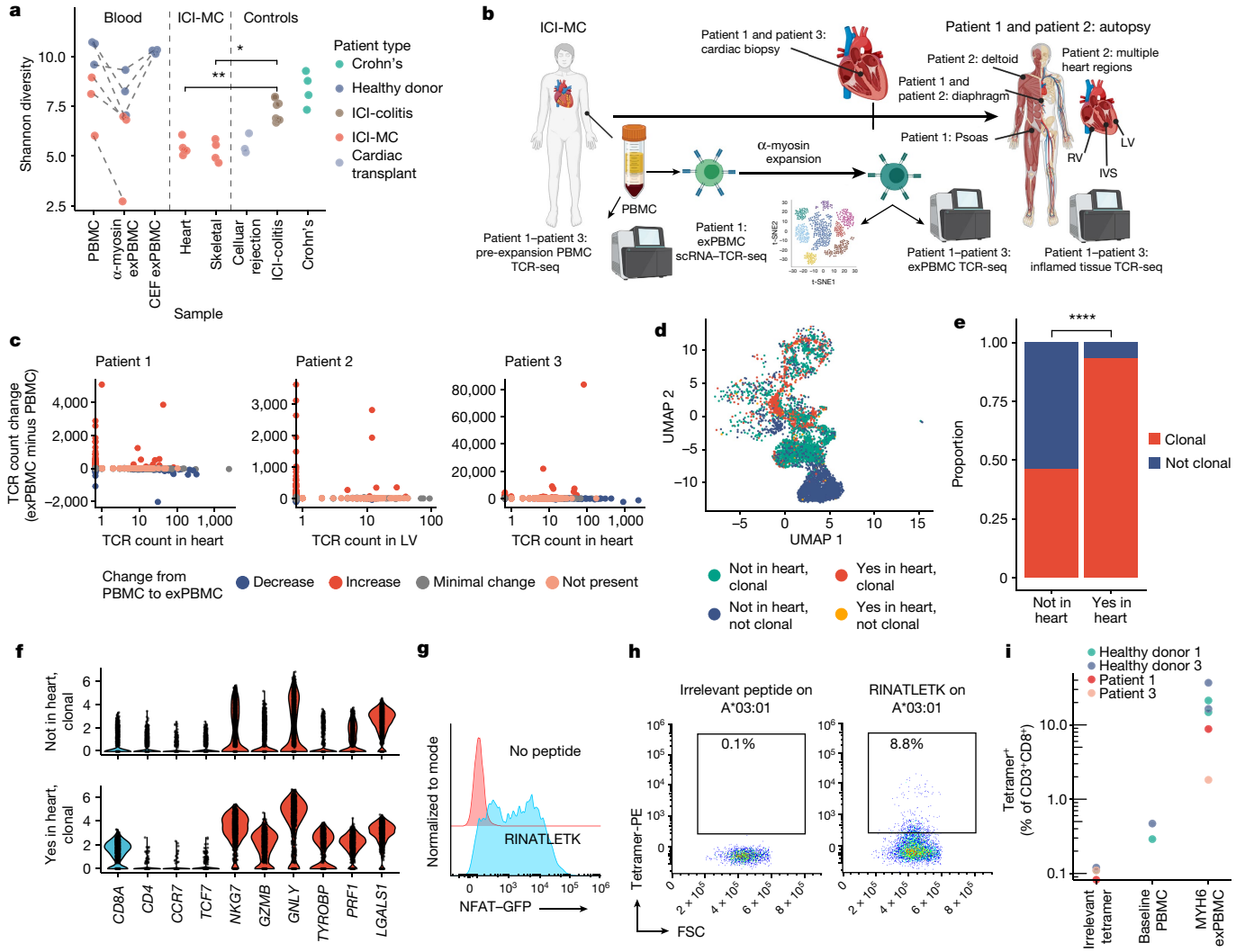

Fig. 4 | α-myosin-expanded TCRs are present in cardiac and skeletal muscle of patients with ICI-MC. a, Shannon diversity of TCR β chain repertoires. Dashed lines connect blood samples within the same donor. *P* values are from two-sided Wilcoxon tests. $n = 6$ PBMCs, $n = 6$ α-myosin exPBMCs, $n = 3$ CEF exPBMCs, $n = 5$ hearts from 3 patients (multiple regions for patient 2), $n = 4$ skeletal muscle from 2 patients, $n = 3$ cellular rejection samples from 3 patients that underwent cardiac transplant, $n = 8$ ICI-associated colitis samples from 8 patients, $n = 4$ Crohn's samples from 4 patients. **b**, Schematic of sampling and analyses of tissues from patients with ICI-MC. IVS, interventricular septum; LV, left ventricle; RV, right ventricle. **c**, Change in TCR counts from PBMCs to α-myosin exPBMCs plotted by abundance of the same TCR β chain in the autologous inflamed cardiac tissue. Minimal change is less than a 50 read count change. Not present means not found in either PBMCs or exPBMCs. **d**, Dimensionality reduction with UMAP on scRNA-seq data of $CD3^+$ exPBMCs derived from patient 1. Groups are divided by whether the TCR β chain expressed by that cell is present in the patient's heart and whether that TCR is clonal (expressed by >2 cells in exPBMCs). **e**, Proportion of single-cell sequenced exPBMCs that are clonal, stratified by whether that TCR is present in the heart. $P < 0.0001$ by two-sided Fisher's exact test. **f**, Violin plots of key genes by the presence or absence in heart and clonality in exPBMCs. Identity genes are in light blue. Naive genes are in dark blue. Activation genes are in red. **g**, Flow cytometry histogram of TCR-Pt1 reporter cell line co-cultured with autologous lymphoblastoid B cell lines and stimulated with 10 μg ml^{-1} RINATLETK peptide relative to no peptide. ($n = 3$ replicates) **h**, Scatter plot showing $CD3^+CD8^+$ exPBMCs from patient 1 stained with irrelevant peptide or RINATLETK on HLA-A:03*01 tetramer. **i**, Quantification of RINATLETK on HLA-A:03*01 tetramer staining across samples compared with the irrelevant peptide. $n = 2$ healthy donors for baseline PBMCs. $n = 6$ exPBMCs (1 replicate for 2 patients with ICI-MC and 2 replicates for 2 healthy donors). Panel **b** was created with BioRender.com.

To assess whether α-myosin-expanded TCR clones might be involved in cardiac and skeletal muscle toxicity, we compared TCR β chain repertoires in the heart and inflamed muscle to those over-represented in α-myosin exPBMCs relative to unexpanded PBMCs. We performed bulk TCR β chain sequencing on formalin-fixed paraffin-embedded tissues from endomyocardial biopsy samples (patients 1 and 3) and autopsy material (patients 1 and 2). Information regarding tissue samples from each patient with myocarditis is summarized in Fig. 4b. High numbers of total TCR reads (>1,500) were obtained in all samples, which was consistent with the observed high T cell infiltration (Extended Data Fig. 6c). Shannon diversity was lower in the hearts and skeletal muscle of patients with ICI-MC compared to inflamed colonic tissue of patients with ICI-associated colitis or Crohn's disease. This result indicates the high clonality of TCR repertoires seen in ICI-MC compared with another immunotherapy-related toxicity associated with high infiltration of T cells[34] (Fig. 4a). Biopsy samples from patients with acute cellular rejection following cardiac transplantation were also included as a cardiac-specific comparison of TCR repertoires. These samples had low Shannon diversity, which provides support for T cell-mediated anticardiac autoimmunity (Fig. 4a).

We plotted the degree of α-myosin expansion (count in α-myosin exPBMCs minus the count in pre-expansion PBMCs) (Fig. 4c and

Extended Data Fig. 8a, with expansion shown in red) against the abundance of the same TCR β chain in the autologous inflamed tissue of patients with ICI-MC. This showed that α-myosin-expanded TCRs are present in inflamed hearts from all three patients (Fig. 4c and Extended Data Fig. 8a). Some α-myosin-expanded TCRs were abundant in the inflamed heart and skeletal muscle (Fig. 4c and Extended Data Fig. 7), which suggested that α-myosin may be a relevant disease antigen for ICI-MC and myositis. We performed scRNA–TCR-seq on sorted $CD3^+$ exPBMCs from patient 1. Gene expression analysis of TCR^+ cells showed expression of *CD3E* in all cells (including cells that expressed both *CD8A* and *CD4*) and a small population of residual B cells that expressed *CD79A* (Extended Data Fig. 8a). We further filtered cells on the basis of a shared TCR β chain with the cardiac TCR repertoire (overlap with bulk β chain sequencing), which would be expected to be enriched for disease-relevant TCRs. Following dimensionality reduction with UMAP, the cells clustered distinctly by group (Fig. 4d). Of the cells with TCR clonotypes shared with the heart, a significantly higher proportion were clonal in exPBMCs relative to cells with TCRs not present in the heart (Fig. 4e). Moreover, these clonal cells had high expression of *CD8A* (Fig. 4f and Extended Data Fig. 8b). Clonal cells in the exPBMCs are expected to be enriched for α-myosin specificity. Clonal cells with TCRs present in the heart also had high expression of markers of activation such as *NKG7*, *GZMB* and *GNLY* (Fig. 4f and Extended Data Fig. 8b).

To confirm that α-myosin expansion generates clonal TCRs specific for α-myosin, we aimed to map the epitope specificity and MHC restriction of a TCR found in both exPBMCs and cardiac tissue of patient 1 (TCR-Pt1) (Extended Data Fig. 9a). HLA types for patients with ICI-MC and healthy donors are shown in Extended Data Table 3. We reconstructed and transduced TCR-Pt1 into Jurkat NFAT–GFP reporter cells (TCR CDR3 and gene information is shown in Table 1). We then used the same approach as for the mouse TCR cell lines for testing against the α-myosin 20-amino-acid peptide library followed by TepiTool-guided epitope narrowing. The results showed that TCR-Pt1 activated the NFAT reporter specifically to $MYH6_{443–451}$ (RINATLETK) (Fig. 4g). This peptide has strong predicted binding to HLA-A*03:01 using TepiTools. In line with this prediction, the TCR-Pt1 cell line stained with a tetramer with $MYH6_{443–451}$ loaded on HLA-A*03:01 but not with a tetramer with the same peptide loaded on HLA-A*24:02 (Extended Data Fig. 9b). Patient 1 carries both of these HLA-A alleles. We next tested $MYH6_{443–451}$ on the A*03:01 tetramer against exPBMCs of healthy donors and patients with ICI-MC bearing HLA-A*03:01. We found a high prevalence of $MYH6_{443–451}$-specific T cells in exPBMCs from patient 1 with ICI-MC and from two healthy donors and low but detectable $MYH6_{443–451}$-specific T cells in exPBMCs from patient 3 with ICI-MC (Fig. 4h,i and Extended Data Fig. 9c). Patient 2 was not assessed because they lacked the HLA-A*03:01 allele. Thus, $CD8^+$ cytotoxic T cells specific for α-myosin are present in the blood and diseased hearts of patients with fulminant ICI-MC and may be present in healthy individuals.

Tumour-specific *MYH6* expression

The importance of α-myosin as an autoantigen in ICI-MC raises the possibility that tumour cells may aberrantly express *MYH6*. Moreover, tumour-reactive T cells specific for α-myosin epitopes may develop and lead to an increased risk for developing ICI-MC. It has been previously reported by our group that a patient with fulminant ICI-MC had aberrant melanoma-specific expression of muscle transcripts, including *MYH6* (ref. [5]). Analyses of a previously published RNA-seq dataset of melanoma tumours treated with ICIs[35] showed that 37 out of 91 tumours expressed low but detectable levels of *MYH6* (Extended Data Fig. 10a). Despite treatment with an ICI, none of these patients developed clinically significant myocarditis or myositis. However, few patients with *MYH6* expression were treated with combination anti-CTLA4 and anti-PD-1, which is a known risk factor for ICI-MC. Given the rarity of myocarditis and the comparatively low patient numbers examined here, these data are insufficient to determine whether tumour-specific *MYH6* expression may be a risk factor for ICI-MC. HLA type may be an important modifying factor. Notably, tumour-specific *MYH6* expression is not unique to this dataset. Analysis of The Cancer Genome Atlas (TCGA) melanoma cohort showed that 250 out of 363 tumours had detectable *MYH6* expression (Extended Data Fig. 10b).

Discussion

Immunotherapy-associated toxicities are important limitations to the use of ICIs. Here we presented a new perspective on ICI-MC as an antigen-driven, cytotoxic T cell-mediated toxicity. We used a genetically altered mouse to model a human drug toxicity and demonstrated that $Pdcd1^{-/-}Ctla4^{+/-}$ mice recapitulate many of the important clinicopathological features of ICI-MC seen in humans, including severe cardiac inflammation predominately composed of $CD8^+$ T cells. The mice also had significant conduction abnormalities and preserved ejection fraction[2]. Animal models that used pharmacological methods have not replicated these important features. MRL mice treated with an anti-PD-1 and an anti-CTLA-4 for 8 weeks develop mild myocarditis that is only evident histologically[2]. Monkeys treated with anti-PD-1 and anti-CTLA-4 antibodies develop mild-to-moderate inflammation in all organs examined, including the heart, in which mild $CD4^+$ T cell infiltration is seen[36].

We showed in our mouse model that myocarditis is characterized by cytotoxic $CD8^+$ T cells with highly clonal TCRs, and that $CD8^+$ cells are necessary for the development of myocarditis. Although CD4 depletion did not rescue survival, it is unknown what part $CD4^+$ T cells play, particularly in the initiation of myocarditis, which is more difficult to determine in a genetic model and is a limitation of our study. The CD8 dependence of our model is in contrast to the CD4 dependence of myocarditis seen in $Pdcd1^{-/-}Lag3^{-/-}$ mice, which raises the possibility of distinct mechanisms of myocarditis with different immune checkpoint deficiencies[37,38]. Three of the most clonal TCRs, derived from independent mice, recognized α-myosin epitopes. Notably, α-myosin-specific TCRs expanded when transferred to recipient mice and occupied >65% of the highly inflamed cardiac TCR repertoire at the time of death from myocarditis. Lack of thymic expression suggests that α-myosin-specific T cells may escape central tolerance mechanisms[3]. α-myosin-specific T cells could be expanded from the blood of healthy donors and of patients with ICI-MC. This finding, which may not be specific to α-myosin, suggests that the presence of α-myosin-specific T cells in the periphery is common in humans. Furthermore, we found that T cells specific for the exact epitope $MYH6_{443–451}$ on HLA-A*03:01 could be expanded from the blood in all four tested samples from patients with the HLA-A*03:01 allele. It is currently unknown whether particular HLA alleles may be a risk factor for ICI-MC. Several studies have recently examined associations of HLA alleles and response or toxicity to ICI[39–42], but more work is needed, particularly for rare toxicities such as myocarditis. In addition, the effect of the microbiome on ICI-MC risk is unknown and should be explored in future work[43,44].

The α-myosin-expanded TCRs overlapped with TCR repertoires in the diseased hearts and skeletal muscle of three patients with ICI-MC. Although the presence of shared clones is insufficient to establish causality, these data suggest that α-myosin may be an important autoantigen in ICI-MC. The presence of other high-frequency TCRs in the hearts that were not enriched in the α-myosin-expanded repertoires could point to other relevant antigens, particularly by the time myocarditis has become severe.

Previous studies have shown that α-myosin is a MHC-II restricted autoantigen in mouse models, primarily using transgenic TCRs or α-myosin vaccination approaches, in which α-myosin is used to initiate an immune response[3,45–50]. Our data here identified MHC-I-restricted α-myosin epitopes in a spontaneous mouse model of myocarditis that

is dependent on CD8$^+$ T cells. Furthermore, we identified a candidate autoantigen for an immunotherapy toxicity in humans. We also identified new specific TCR-peptide–MHC interactions for three mouse TCRs and one human TCR. Knowledge of the most relevant disease antigens may facilitate antigen-directed approaches to suppress inflammation without compromising on antitumour efficacy such as tolerogenic vaccines. Identification of α-myosin as an autoantigen may also guide the identification of biomarkers to predict which patients are at higher risk for myocarditis, such as surveillance of peripheral α-myosin-reactive T cells or identification of pre-existing autoantibodies.

Online content

Any methods, additional references, Nature Research reporting summaries, source data, extended data, supplementary information, acknowledgements, peer review information; details of author contributions and competing interests; and statements of data and code availability are available at https://doi.org/10.1038/s41586-022-05432-3.

1. Wang, D. Y. et al. Fatal toxic effects associated with immune checkpoint inhibitors: a systematic review and meta-analysis. *JAMA Oncol.* **4**, 1721–1728 (2018).
2. Wei, S. C. et al. A genetic mouse model recapitulates immune checkpoint inhibitor-associated myocarditis and supports a mechanism-based therapeutic intervention. *Cancer Discov.* **11**, 614–639 (2020).
3. Lv, H. et al. Impaired thymic tolerance to α-myosin directs autoimmunity to the heart in mice and humans. *J. Clin. Invest.* **121**, 1561–1573 (2011).
4. Gabrielsen, I. S. M. et al. Transcriptomes of antigen presenting cells in human thymus. *PLoS ONE* **14**, e0218858 (2019).
5. Johnson, D. B. et al. Fulminant myocarditis with combination immune checkpoint blockade. *N. Engl. J. Med.* **375**, 1749–1755 (2016).
6. Hu, J.-R. R. et al. Cardiovascular toxicities associated with immune checkpoint inhibitors. *Cardiovasc. Res.* **115**, 854–868 (2019).
7. Salem, J. E. et al. Spectrum of cardiovascular toxicities of immune checkpoint inhibitors: a pharmacovigilance study. *Lancet Oncol.* **19**, 1579–1589 (2018).
8. Moslehi, J., Lichtman, A. H., Sharpe, A. H., Galluzzi, L. & Kitsis, R. N. Immune checkpoint inhibitor–associated myocarditis: manifestations and mechanisms. *J. Clin. Invest.* https://doi.org/10.1172/JCI145186 (2021).
9. Zamami, Y. et al. Factors associated with immune checkpoint inhibitor-related myocarditis. *JAMA Oncol.* **5**, 1635–1637 (2019).
10. Salem, J.-E. et al. Abatacept for severe immune checkpoint inhibitor-associated myocarditis. *N. Engl. J. Med.* **380**, 2377–2379 (2019).
11. Yang, X., Bam, M., Becker, W., Nagarkatti, P. S. & Nagarkatti, M. Long noncoding RNA AW112010 promotes the differentiation of inflammatory T cells by suppressing IL-10 expression through histone demethylation. *J. Immunol.* **205**, 987–993 (2020).
12. Jackson, R. et al. The translation of non-canonical open reading frames controls mucosal immunity. *Nature.* **564**, 434–438 (2018).
13. Adamo, L. et al. Myocardial B cells are a subset of circulating lymphocytes with delayed transit through the heart. *JCI Insight* https://doi.org/10.1172/jci.insight.134700 (2020).
14. Bönner, F., Borg, N., Burghoff, S. & Schrader, J. Resident cardiac immune cells and expression of the ectonucleotidase enzymes CD39 and CD73 after ischemic injury. *PLoS ONE* https://doi.org/10.1371/journal.pone.0034730 (2012).
15. Martini, E. et al. Single-cell sequencing of mouse heart immune infiltrate in pressure overload-driven heart failure reveals extent of immune activation. *Circulation.* **140**, 2089–2107 (2019).
16. Li, O., Zheng, P. & Liu, Y. CD24 expression on T cells is required for optimal T cell proliferation in lymphopenic host. *J. Exp. Med.* **200**, 1083–1089 (2004).
17. Hubbe, M. & Altevogt, P. Heat-stable antigen/CD24 on mouse T lymphocytes: evidence for a costimulatory function. *Eur. J. Immunol.* **24**, 731–737 (1994).
18. Szabo P. A., Miron M. & Farber D. L. Location, location, location: tissue resident memory T cells in mice and humans. *Sci. Immunol.* https://doi.org/10.1126/sciimmunol.aas9673 (2019).
19. Fonseca, R. et al. Runx3 drives a CD8$^+$ T cell tissue residency program that is absent in CD4$^+$ T cells. *Nat. Immunol.* **23**, 1236–1245 (2022).
20. Zhang, L. et al. Major adverse cardiovascular events and the timing and dose of corticosteroids in immune checkpoint inhibitor-associated myocarditis. *Circulation* **141**, 2031–2034 (2020).
21. Coutinho, A. E. & Chapman, K. E. The anti-inflammatory and immunosuppressive effects of glucocorticoids, recent developments and mechanistic insights. *Mol. Cell. Endocrinol.* **335**, 2–13 (2011).
22. Heather, J. M. et al. Stitchr: stitching coding TCR nucleotide sequences from V/J/CDR3 information. *Nucleic Acids Res.* **1**, e68 (2022).
23. Rosskopf, S. et al. A Jurkat 76 based triple parameter reporter system to evaluate TCR functions and adoptive T cell strategies. *Oncotarget* **9**, 17608–17619 (2018).
24. Jutz, S. et al. Assessment of costimulation and coinhibition in a triple parameter T cell reporter line: simultaneous measurement of NF-κB, NFAT and AP-1. *J. Immunol. Methods.* **430**, 10–20 (2016).
25. Gil-Cruz, C. et al. Microbiota-derived peptide mimics drive lethal inflammatory cardiomyopathy. *Science* **366**, 881–886 (2019).
26. Massilamany, C., Gangaplara, A., Steffen, D. & Reddy, J. Identification of novel mimicry epitopes for cardiac myosin heavy chain-α that induce autoimmune myocarditis in A/J mice. *Cell Immunol.* **271**, 438–449 (2011).
27. Meier, S. L., Satpathy, A. T. & Wells, D. K. Bystander T cells in cancer immunology and therapy. *Nat. Cancer* **3**, 143–155 (2022).
28. Maurice, N. J., McElrath, M. J., Andersen-Nissen, E., Frahm, N. & Prlic, M. CXCR3 enables recruitment and site-specific bystander activation of memory CD8$^+$ T cells. *Nat. Commun.* **10**, 1–15 (2019).
29. Simoni, Y. et al. Bystander CD8$^+$ T cells are abundant and phenotypically distinct in human tumour infiltrates. *Nature* **557**, 575–579 (2018).
30. Maurice, N. J., Taber, A. K. & Prlic, M. The ugly duckling turned to swan: a change in perception of bystander-activated memory CD8 T Cells. *J. Immunol.* **206**, 455–462 (2021).
31. Scheper, W. et al. Low and variable tumor reactivity of the intratumoral TCR repertoire in human cancers. *Nat. Med.* **25**, 89–94 (2019).
32. Paul, S., Sidney, J., Sette, A. & Peters, B. TepiTool: a pipeline for computational prediction of T cell epitope candidates. *Curr. Protoc. Immunol.* **2016**, 18.19.1–18.19.24 (2016).
33. Falk, K., Rötzschke, O., Stevanović, S., Jung, G. & Rammensee, H. G. Allele-specific motifs revealed by sequencing of self-peptides eluted from MHC molecules. *Nature* **351**, 290–296 (1991).
34. Luoma, A. M. et al. Molecular pathways of colon inflammation induced by cancer immunotherapy. *Cell* **182**, 655–671.e22 (2020).
35. Johnson, D. B. et al. Tumor-specific MHC-II expression drives a unique pattern of resistance to immunotherapy via LAG-3/FCRL6 engagement. *JCI Insight* **3**, e120360 (2018).
36. Ji, C. et al. Myocarditis in cynomolgus monkeys following treatment with immune checkpoint inhibitors. *Clin. Cancer Res.* **25**, 4735–4748 (2019).
37. Woo, S. R. et al. Immune inhibitory molecules LAG-3 and PD-1 synergistically regulate T-cell function to promote tumoral immune escape. *Cancer Res.* **72**, 917–927 (2012).
38. Okazaki, T. et al. PD-1 and LAG-3 inhibitory co-receptors act synergistically to prevent autoimmunity in mice. *J. Exp. Med.* **208**, 395–407 (2011).
39. Chowell, D. et al. Patient HLA class I genotype influences cancer response to checkpoint blockade immunotherapy. *Science* **359**, 582–587 (2018).
40. Naranbhai, V. et al. *HLA-A*03* and response to immune checkpoint blockade in cancer: an epidemiological biomarker study. *Lancet Oncol.* https://doi.org/10.1016/S1470-2045(21)00582-9 (2022).
41. Correale, P. et al. HLA expression correlates to the risk of immune checkpoint inhibitor-induced pneumonitis. *Cells* https://doi.org/10.3390/cells9091964 (2020).
42. Hasan Ali, O. et al. Human leukocyte antigen variation is associated with adverse events of checkpoint inhibitors. *Eur. J. Cancer* **107**, 8–14 (2019).
43. McCulloch, J. A. et al. Intestinal microbiota signatures of clinical response and immune-related adverse events in melanoma patients treated with anti-PD-1. *Nat. Med.* https://doi.org/10.1038/s41591-022-01698-2 (2022).
44. Andrews, M. C. et al. Gut microbiota signatures are associated with toxicity to combined CTLA-4 and PD-1 blockade. *Nat. Med.* https://doi.org/10.1038/s41591-021-01406-6 (2021).
45. Van der Borght, K. et al. Myocarditis elicits dendritic cell and monocyte infiltration in the heart and self-antigen presentation by conventional type 2 dendritic cells. *Front. Immunol.* **9**, 2714 (2018).
46. Rieckmann, M. et al. Myocardial infarction triggers cardioprotective antigen-specific T helper cell responses. *J. Clin. Invest.* https://doi.org/10.1172/jci123859 (2019).
47. Lee, J. H. et al. Myosin-primed tolerogenic dendritic cells ameliorate experimental autoimmune myocarditis. *Cardiovasc. Res.* **101**, 203–210 (2014).
48. Tajiri, K. et al. A new mouse model of chronic myocarditis induced by recombinant Bacille Calmette–Guèrin expressing a T-cell epitope of cardiac myosin heavy chain-α. *Int. J. Mol. Sci.* **22**, 794 (2021).
49. Hua, X. et al. Single-cell RNA sequencing to dissect the immunological network of autoimmune myocarditis. *Circulation* https://doi.org/10.1161/circulationaha.119.043545 (2020).
50. Taylor, J. A. et al. A spontaneous model for autoimmune myocarditis using the human MHC molecule HLA-DQ8. *J. Immunol.* **172**, 2651–2658 (2004).

Methods

Mice

Pdcd1$^{-/-}$*Ctla4*$^{+/-}$ mice were maintained as previously described[2]. Female mice were primarily (but not exclusively) used in these studies owing to their higher incidence of myocarditis. *Rag1*$^{-/-}$ mice were purchased from The Jackson Laboratory (002216)[51]. For the generation of survival curves, events were defined as either death (that is, mice found dead) or identification of mice that required euthanasia (for example, due to lethargy, moribund, dyspnoea or weight loss). All mice were housed at Vanderbilt University Medical Center vivarium, an animal facility accredited by the Association for Assessment and Accreditation of Laboratory Animal Care International and is specific pathogen-free. All experiments were performed in accordance with Vanderbilt University Medical Center Institutional Animal Care and Use Committee guidelines. No blinding was used in the studies. Where possible, mice were randomized to treatment groups or study arms. Mice were on 12-h light–dark cycles, which coincided with daylight hours in Nashville, TN, United States. The mouse housing facility was maintained at 20–25 °C and 30–70% humidity.

Preparation of cardiac dissociates for scRNA–TCR-seq

Single-cell suspensions were obtained from mouse hearts by mincing followed by enzymatic digestion with 125 U ml^{-1} DNase I (Worthington, LS002138) and 250 U ml^{-1} collagenase 3 (Worthington, LS004182). Dissociated hearts were filtered through a 30-µm filter. Red blood cells were lysed using ACK lysing buffer (KD Medical/MediaTech, NC0274127). Single-cell suspensions were either used fresh or cryopreserved in 10% DMSO with 90% FBS. Before sorting, cells were stained with Alex Fluor 488 (AF488) anti-mouse CD45 (BioLegend, clone 30-F11, 103122; dilution 1:1,000) for 20 min at 4 °C. Following staining and washing with PBS, cells were resuspended in PBS with DAPI (1:20,000). Live CD45^{+} immune cells were sorted by FACS on AF488-positive DAPI-negative events. The wild-type control sample consisted of pooled, without hashing, cardiac immune infiltrates from six female mice to obtain sufficient cells, as the healthy heart has a low frequency of cardiac immune cells. The myocarditis sample consisted of four inflamed hearts from female *Pdcd1*$^{-/-}$*Ctla4*$^{+/-}$ mice. Inflammation was confirmed by flow cytometry for CD45. Only mice with CD45^{+} cells constituting >10% of the total single cells were included. Mice ranged from 3 to 6 weeks in age. One inflamed heart was run as an individual sample on a 10x Genomics chromium platform. The additional three inflamed hearts were hashed together using Total Seq C reagents according to the manufacturer's instructions (BioLegend, TotalSeq-C0301, 155861; TotalSeq-C0302, 155863; TotalSeq-C0303, 155865).

scRNA–TCR-seq

Each sample (targeting 5,000–15,000 cells per sample) was processed for single-cell 5′ RNA and TCR sequencing utilizing the 10x Chromium system. Libraries were prepared following the manufacturer's protocol. The libraries were sequenced using NovaSeq 6000 with 150 bp paired-end reads. RTA (v.2.4.11; Illumina) was used for base calling, and analysis was completed using 10x Genomics Cell Ranger software. Data were analysed in R using the filtered h5 gene matrices in the Seurat package[52–54]. In brief, samples were subset to include cells with >200 but <3,000 unique transcripts to exclude probable non-cellular RNA reads and doublets. Cells with >15% of reads coming from mitochondrial transcripts were also excluded as probable dying cells. For mouse hearts, hash tag oligonucleotides were deconvoluted using HTODemux, with the positive quantile set at 0.85. Samples were downsized so that equivalent numbers of cells originating from healthy wild-type or myocarditis *Pdcd1*$^{-/-}$*Ctla4*$^{+/-}$ cardiac-infiltrating immune cells were included (2,509 cells per genotype of origin). Ten clusters were identified using a resolution of 0.4. UMAP was used for dimensionality reduction with 15 nearest neighbours and minimum distance of 0.5. SingleR was used to assist with cell-type annotation of clusters. Clonal is defined as more than two cells with the same TCR clonotype (defined by unique combinations of CDR3 regions). T cells were subset on the expression level of *Cd3e* >1.5 and presence of a TCR (n = 1,266 cells). Clustering with the Louvain algorithm at resolution of 0.3 produced five distinct clusters. Additional subclustering produced small clusters of <15 cells. Differential gene expression analyses were used to identify clusters. TCR density is defined as the number of the 100 nearest cell neighbours expressing the same TCR clonotype (α and β chain).

TCR-seq

TCR-seq and clonality quantification was assessed in formalin-fixed paraffin embedded (FFPE) or snap-frozen samples of mouse hearts or spleens. All human samples were derived from FFPE samples or isolated PBMCs. For FFPE samples, RNA was extracted from 10-µm sections using Promega Maxwell 16 FFPE RNA kits per the manufacturer's protocol. TCRs were sequenced using the TCR Immunoverse all chain assay per the manufacturer's protocol (Invitae/ArcherDX). Sequencing results were evaluated using Archer Immunoverse analyser. CDR3 sequences and frequency tables were extracted from the manufacturers' analysis platform and imported into R for analysis using the Immunarch package (https://immunarch.com) in R.

Antibody-mediated depletion and dexamethasone treatment

Female *Pdcd1*$^{-/-}$*Ctla4*$^{+/-}$ mice were randomly assigned to control or dexamethasone treatment at 21 days of age. Mice were treated with 1 mg kg^{-1} day^{-1} of dexamethasone. Experiments were concluded when mice reached 115 days of age. Female *Pdcd1*$^{-/-}$*Ctla4*$^{+/-}$ mice were randomly assigned to control, anti-CD8a or anti-CD4 injections at 21 days of age. Mice were intraperitoneally injected three times a week with 200 µg of anti-CD4 (BioXCell, BE0003-1, clone GK1.5) or anti-CD8 (BioXCell, BE0061, clone 2.43) antibodies or vehicle, all in a maximum volume of 100 µl. Treatment lasted until 90 days of age. Peripheral blood was sampled by tail prick for assessment of depletion efficiency at week 3. To detect an anticipated mortality difference of 50% (for control) to 5% (for an intervention that reduces mortality) with an α of 0.05 and 80% power, a sample size of 14 mice per group was needed.

Adoptive transfer

Splenocytes were isolated from *Pdcd1*$^{-/-}$*Ctla4*$^{+/-}$ mice with myocarditis by manual dissociation, filtering and red blood cell lysis. Myocarditis of the donor mice was confirmed by either haematoxylin and eosin (H&E) staining or dissociation of the heart and flow cytometry for CD45^{+} immune cells. A portion of each spleen underwent CD8 depletion using magnetic bead isolation (Miltenyi CD8 (TIL) MicroBeads, mouse, 130-116-478). One million whole or CD8-depleted splenocytes were injected into each *Rag1*$^{-/-}$ recipient mouse in 100 µl PBS through tail vein injection. Mice were monitored for death or signs of distress. At death or euthanasia, hearts, spleens, livers, lungs and kidneys were stained by H&E and evaluated by microscopy. To detect an anticipated mortality difference of 50% (for whole splenocyte transfer) to 1% (for CD8-depleted splenocyte transfer) with an α of 0.05 and 80% power, a sample size of 11 mice per group was needed.

Histology and pathology

Formalin-fixed tissues were processed routinely into paraffin blocks, sectioned at 5 µm and stained with H&E using standard protocols at Vanderbilt University Medical Center's Translational Pathology Shared Resource (TPSR) core laboratory. To further characterize the mononuclear cardiac infiltrates detected by light microscopy, a panel of IHC markers was used. IHC staining was performed at the TPSR using standard, validated protocols for chromogenic IHC. All steps besides dehydration, clearing and coverslipping were performed on a Leica Bond-Max IHC autostainer (Leica Biosystems). Slides were deparaffinized. Antigen retrieval was performed using EDTA (CD markers) or

proteinase K (F4/80) or on the Bond Max using their Epitope Retrieval 2 solution for 20 min (CD45R and IgG). Slides were incubated with primary antibodies as indicated below. Secondary antibody labelling was performed for all markers except CD3 and IgG by incubating in rabbit anti-rat antibody (BA-4001, Vector Laboratories) for 15 min at a 1:650 dilution. Immunolabelling by rabbit antibody was visualized using a Bond polymer refine detection system (DS9800, Leica Biosystems). Slides were then dehydrated, cleared and coverslipped. For primary antibodies, anti-CD3 (Abcam, Ab16669) was used at 1:250 dilution, anti-CD4 (eBioscience, 14–9766–82) was used at 1:1,000 dilution, anti-CD8 (eBioscience, 14–0808–82) was used at 1:1,000 dilution, anti-F4/80 (Novus Biologicals, NB600–404) was used at 1:900 dilution and anti-CD45R/B220 (553086, BD Pharmingen, clone RA3-6B2) was used at 1:20,000 dilution. For IgG, slides were placed in a Biotin Blocking system (x0590, Dako) for 10 min each. Slides were incubated in biotinylated goat anti-mouse IgG (BA-9200, Vector Laboratories) for 15 min at 1:2,000 dilution. A Bond Intense R detection system (DS9263, Leica Biosystems) was used for visualization. IHC quantification is reported as number of positive cells per high power field (×40), averaged over three high power fields per slide. Slide images were obtained using Olympus cellSens Standard v.1.17.

RNA preparation and quantitative PCR analysis

Flash-frozen mouse tissue (cardiac ventricle or thymus) was homogenized using a TissueLyser II (Qiagen) for 2 min at 30 Hz. RNA was collected from dissociated tissue using a Maxwell 16 automated workstation (Promega) and a LEV simplyRNA Tissue kit (Promega, AS1280). RNA was then analysed for concentration using a NanoDrop 2000 (Thermo Fisher Scientific) before cDNA synthesis using a SensiFAST cDNA Synthesis kit (Bioline, Meridian Bioscience, BIO-65054) with 1 μg of RNA per sample. cDNA and SsoAdvanced Universal SYBR Green Supermix (Bio-Rad, 1725270) were then combined with target-specific primers on a CFX96 Touch Real-Time PCR Detection system (Bio-Rad). The following primer pairs were used: *Sbk2* forward 5′-CTCTGAGCCCAGAAATGCCA-3′ reverse 5′-AATGTGTTCCAGGGCAGAGG-3′; *Nppb* forward 5′-CGTTTGGGCTGTAACGCACTG-3′ reverse 5′-TCACTTCAAAGGTGGTCCCAG-3′; *Nppa* forward 5′-TCTGATGGATTTCAAGAACCTGCT-3′ reverse 5′-ACACACCACAAGGGCTTAGG-3′; *Myh6* forward 5′-AACCAGAGTTTGAGTGACAGAATG-3′ reverse 5′-ACTCCGTGCGGATGTCAA-3′; *Actb* forward 5′-ACGGCCAGGTCATCACTATTG-3′ reverse 5′-AGGATTCCATACCCAAGAAGGAA-3′. Three technical replicates were used for each reaction. *Actb* (encoding β-actin) was used as the housekeeping gene. Data were analysed using the ΔC_t method in which the number of cycles needed to amplify the gene of interest is normalized to the number of cycles needed to amplify the housekeeping gene.

Flow cytometry for mouse cell populations and Jurkat reporter cells

Samples were run on an Attune NxT Acoustic Focusing cytometer (Life Technologies). Data were collected using Attune NxT software v.3.2.1. Analysis was performed in FlowJo v.10.6. Gating was first done on forward scatter and side scatter to exclude debris. Doublets were excluded by gating on FSC area versus FSC height. DAPI was used to exclude dead cells from analyses. The following antibodies were used: CD45-PerCP/Cy5.5 (BioLegend, 103132, clone 30-F11; dilution 1:400); CD3-AF488 (BioLegend, 100210, clone 17A2; dilution 1:200); CD4-APC (BioLegend, 100412, clone GK1.5; dilution 1:100); CD8a-PE/Cy7 (BioLegend, 100722, clone 53-6.7; dilution 1:400); Thy1.1 (BioLegend, 202506, clone OX-7; dilution 1:1,000 for AF488, 1:500 for APC/Cy7); and TCR β chain-PE (BioLegend, 109208, clone H57–597; dilution 1:200). All cell lines were routinely tested and confirmed to be clear of mycoplasma contamination.

TCR sequences and cloning

TCR sequences were generated from CDR3 regions, V genes and J genes using Stitchr[22]. Paired TCR α and β sequences were derived from single-cell sequencing or from the adoptive transfer experiments in which pairing of chains could be inferred from bulk sequencing as single α and β chains made up the majority of each repertoire. Genes for α and β chains were separated using a T2A sequence. Restriction digest sites were added to either end. Full TCR gene blocks were synthesized as custom orders from Genewiz. Full TCR block sequences can be found in Supplementary Information. TCR sequences were cloned into a MSCV-IRES-Thy1.1 DEST vector. MSCV-IRES-Thy1.1 DEST was a gift from A. Rao (Addgene plasmid 17442; RRID: Addgene_17442)[55]. Retrovirus was made using the platA retroviral packaging cell line (Cell BioLabs RV-102). Jurkat-TCR-ko-CD8$^+$-NFAT-GFP reporter cells were a gift from P. Steinberger. Reporter cells were retrovirally transduced with TCRs of interest. TCR expression was confirmed by flow cytometry for Thy1.1 and TCR β chain. Retrovirally transduced cells were sorted on a WOLF cell sorter (NanoCellect) for Thy1.1-AF488. Cells were confirmed to be >90% Thy1.1-positive after sorting before use in downstream assays.

Antigen discovery

Jurkat-NFAT–GFP cell lines with reconstructed TCRs were used for antigen screening. Syngeneic (derived from C57BL/6 mice) BMDCs were used as APCs. BMDCs were generated by flushing femurs and tibias from mice with PBS, filtering the cells though a 70-μm filter, lysing red blood cells and plating in RMPI medium with 10% FBS, 1% HEPES and 20 ng ml^{-1} GM-CSF (ProSpec, CYT-222). BMDCs were polarized in GM-CSF-containing medium for 9 days (replacing the medium at days 3 and 6) before collecting the adherent fraction through mechanical dissociation using a cell scraper and cryopreservation for subsequent experiments. For antigen discovery, BMDCs were thawed into GM-CSF-containing medium in flat-bottom plates the day before adding TCR cell lines and peptides. Cells were plated at a ratio of 1 TCR cell to 3 BMDCs. The α-myosin, ANP, BNP and SBK2 peptide library was generated as 20-amino-acid peptides with 5-amino-acid overlaps from GenScript. Owing to insolubility in aqueous solution, two 20-amino-acid peptides were replaced by three 10-amino-acid peptides each. Sequences of all 172 peptides are shown in Extended Data Table 1. Peptides were added at a concentration of 10 μg ml^{-1}, and co-cultures were incubated overnight. TCR cell lines were stained with DAPI to assess viability and analysed by flow cytometry for NFAT–GFP reporter activity. For the human TCR (TCR-Pt1), autologous lymphoblastoid B cell lines (LCLs) were used as APCs. TCR-Pt1 was screened against 130 α-myosin peptides.

MHC blockade

Jurkat TCR cell lines were co-cultured with EL-4 cells as APCs with or without 10 μg ml^{-1} cognate peptide overnight. EL-4 cells were a gift from S. Mallal. Blocking antibodies (anti-Db clone 28-14-8S or anti-Kb clone B8-24-3) were added to cells at a concentration of 10 μg ml^{-1} for 1 h before adding peptides. Blocking antibodies were provided by J. Sidney. TCR cell lines were stained with Thy1.1-APC/Cy7 (BioLegend, 202506, clone OX-7; dilution 1:500) to differentiate from EL-4s and with DAPI to assess viability and analysed by flow cytometry for NFAT–GFP reporter activity.

Patients

All studies were conducted in accordance with the Declaration of Helsinki principles under protocols approved by the Vanderbilt University Medical Center Institutional Review Board. Healthy donors provided informed consent under an institutionally approved protocol (IRB number 030062). Patients with myocarditis and family members provided informed consent for research use of biospecimens and clinical data (IRB number 191213). Patients with ICI-associated colitis and patients with Crohn's disease provided informed consent for research use of biospecimens and clinical data (IRB number 09109). Patients that underwent a cardiac transplant and patients with heart failure provided informed consent for research use of biospecimens and clinical data (IRB number 200551). Information regarding patients

that formed the RNA-seq cohort has been previously published[35]. An additional melanoma gene expression dataset was generated by The Cancer Genome Atlas Research Network (https://www.cancer.gov/tcga) and accessed using cBioPortal[56,57].

Generation of LCLs from PBMCs

Epstein–Barr virus (EBV)-transformed LCLs were generated from cryopreserved donor PBMCs by infection with EBV virus stock[58,59]. Approximately 1–3 × 10^6 PBMCs in RPMI-1640 medium supplemented with non-heat-inactivated 20% FBS, 1 µg ml^{-1} cyclosporin A (Sigma-Aldrich, C1832) and 2.5 µg ml^{-1} CpG (Invitrogen, ODN2006) were infected with filtered EBV stock and cultured for 2–3 weeks until clusters of cells were visible by light microscopy. All cell lines were routinely tested and confirmed to be clear of mycoplasma contamination.

PBMC expansion

PBMCs were isolated from EDTA collection tubes and processed using a Ficoll gradient. Antigen-specific PBMC expansion was adapted from previously described protocols[60,61]. Fresh or cryopreserved PBMCs were stimulated with 130 pooled α-myosin peptides at a final concentration of 400 ng ml^{-1} of each peptide or a pool of control CEF peptides (AnaSpec, AS-61036-003). PBMCs were cultured in CTS OpTmizer medium (CTS OpTmizer T Cell Expansion SFM with CTS supplement A1048501, substituted with 2 mM L-glutamine and 2% human serum, Sigma-Aldrich, H3667) with cytokine supplementation (25 ng ml^{-1} each of rhIL-2, rhIL-7 and rhIL-15, Peprotech). For patients with myocarditis (patients 1, 2 and 3), expansion cultures were also supplemented with autologous LCLs to serve as APCs at a ratio of 1 APC per 10 PBMCs. For healthy donors, expansion was done directly from fresh, not cryopreserved, blood. Peptides were only added on the first day of culture. On day 3, additional medium with cytokines was added. On day 7, cells were transferred to a new culture dish with fresh medium with cytokines. Cells were analysed or cryopreserved on day 14.

Single-cell sequencing of exPBMCs

exPBMCs from patient 1 were prepared for single-cell sequencing as follows. exPBMCs were incubated with Human TruStain FcX (Fc receptor blocking solution, BioLegend, 422302; dilution 1:100) for 5 min on ice. Cells were then washed and incubated with human anti-CD3-AF488 (BioLegend, 300319, clone HIT3a; dilution 1:200) for 30 min on ice, and then washed and resuspended to a concentration of 5 × 10^5 cells per ml. SYTOX AADvanced Ready Flow reagent (Invitrogen, R37173, dilution 2 drops per 1 ml) was used per the manufacturer's instructions to exclude dead cells. $CD3^+$ live cells were sorted on a WOLF cell sorter (Nanocellect). Cells were sequenced and data were analysed as described above. Data were analysed in R using the filtered h5 gene matrices in the Seurat package[52–54]. In brief, samples were subset to include cells with >200 but <4,000 unique transcripts to exclude probable non-cellular RNA reads and doublets. Cells with >15% of reads coming from mitochondrial transcripts were also excluded as probable dying cells. Clonal is defined as more than two cells with the same TCR clonotype (defined by specific combinations of CDR3 regions). For exPBMCs, 5,816 cells with TCR reads were analysed. To identify TCRs overlapping with the cardiac repertoire, β CDR3 sequences were used.

Tetramer staining and flow cytometry

Mouse tetramer staining was done using an empty H-2Kb-PE tetramer (Tetramer Shop). Empty tetramer was loaded with peptide by incubating 5 µl of empty tetramer with 0.5 µl of 200 µM peptide solution (all peptides were custom ordered from GenScript, in this case VIQYFASI, VQQVYYSI or SIINFEKL as an irrelevant peptide control, which is known to strongly bind to H-2Kb) for at least 30 min at 4 °C. Loaded tetramers were centrifuged at 3,300*g* for 5 min before use. Mouse hearts were dissociated as described above. Cells were first stained with Zombie Violet (BioLegend, 423113; dilution 1:1,000) for 15 min at room temperature in PBS with no added protein. Cells were then incubated with TruStain FcX block (BioLegend, 101319, clone 93; dilution 1:100) for 5 min at room temperature. Cells were washed in PBS with 2% FBS. Cells were stained with 5 µl of loaded tetramer in 50 µl PBS with 2% FBS for 20 min at 37 °C. Without washing, 20 µl of solution containing the desired surface antibodies was added and cells were incubated for 20 min at 4 °C. The following surface antibodies used: anti-CD3-APC (BioLegend, 100235, clone 17A2; dilution 1:400) and anti-CD8a-FITC (Thermo Fisher, MA5–16759, clone KT15; dilution 1:200). Samples were washed and then analysed.

Human tetramer staining was done using empty tetramers easYmer HLA-A*03:01 (Eagle Biosciences, 1016-01-20) or easYmer HLA-A*24:02 (Eagle Biosciences, 1020-01-20). Monomers were loaded with peptide per the manufacturer's instructions and incubated for 48 h at 18 °C. Tetramers were produced by adding 2.1 µl of streptavidin–PE antibody (BioLegend, 405203) and incubating for at least 1 h at 4 °C. Cells were first stained with Zombie Violet (BioLegend, 423113; dilution 1:1,000) for 15 min at room temperature in PBS with no added protein. Cells were then incubated with TruStain FcX block (BioLegend, 422301; dilution 1:200). Cells were stained with tetramer in PBS with 2% FBS for 20 min at room temperature. Cells were then washed and stained with the surface antibodies anti-CD3-AF488 (BioLegend, 300319, clone HIT3a; dilution 1:200) and anti-CD8a-APC (BioLegend, 301014, clone RPA-T8; dilution 1:200) for 20 min at 4 °C. Samples were washed in PBS with 2% FBS. Samples were run on an Attune NxT Acoustic Focusing cytometer (Life Technologies). Analysis was performed in FlowJo. Gating was first done on forward scatter and side scatter to exclude debris. Doublets were excluded by gating on FSC area versus FSC height. Zombie Violet was used to exclude dead cells from analyses.

Statistical analysis

All statistical analyses were performed in R v.4.1.1. All single-cell statistical analyses were calculated in R using the Seurat package[52–54]. Visualization and graph generation was performed in R. Shannon diversity was calculated using the R package vegan[62]. The R package immunarch was used for evaluating TCR repertoires[63]. *P* value cut-offs displayed on plots correspond to not significant (NS; $P > 0.05$), $^*P < 0.05$, $^{**}P < 0.01$, $^{***}P < 0.001$ and $^{****}P < 0.0001$.

Reporting summary

Further information on research design is available in the Nature Portfolio Reporting Summary linked to this article.

Data availability

Sequencing data have been deposited in the Gene Expression Omnibus under accession number GSE213486. Source data are provided with this paper.

51. Mombaerts, P. et al. RAG-1-deficient mice have no mature B and T lymphocytes. *Cell* **68**, 869–877 (1992).
52. Satija, R., Farrell, J. A., Gennert, D., Schier, A. F. & Regev, A. Spatial reconstruction of single-cell gene expression data. *Nat. Biotechnol.* **33**, 495–502 (2015).
53. Butler, A., Hoffman, P., Smibert, P., Papalexi, E. & Satija, R. Integrating single-cell transcriptomic data across different conditions, technologies, and species. *Nat. Biotechnol.* **36**, 411–420 (2018).
54. Stuart, T. et al. Comprehensive integration of single-cell data. *Cell.* **177**, 1888–1902.e21 (2019).
55. Wu, Y. et al. FOXP3 controls regulatory T cell function through cooperation with NFAT. *Cell.* **126**, 375–387 (2006).
56. Gao, J. et al. Integrative analysis of complex cancer genomics and clinical profiles using the cBioPortal. *Sci. Signal.* https://doi.org/10.1126/scisignal.2004088 (2013).
57. Cerami, E. et al. The cBio cancer genomics portal: an open platform for exploring multidimensional cancer genomics data. *Cancer Discov.* **2**, 401–404 (2012).
58. Oh, H. M. et al. An efficient method for the rapid establishment of Epstein-Barr virus immortalization of human B lymphocytes. *Cell Prolif.* **36**, 191–197 (2003).
59. Granato, M. et al. Epstein–Barr virus blocks the autophagic flux and appropriates the autophagic machinery to enhance viral replication. *J. Virol.* **88**, 12715 (2014).
60. Wölfl, M. & Greenberg, P. D. Antigen-specific activation and cytokine-facilitated expansion of naive, human $CD8^+$ T cells. *Nat. Protoc.* **9**, 950–966 (2014).

61. Eberhardt, C. S. et al. Functional HPV-specific PD-1^{+} stem-like CD8 T cells in head and neck cancer. *Nature* **597**, 279–284 (2021).
62. Oksanen, J. et al. vegan: Community Ecology Package. R package version 2.5-7 (2020).
63. Nazarov, V., immunarch.bot, Rumynskiy, E. immunomind/immunarch: 0.6.5: Basic single-cell support. *Zenodo* https://doi.org/10.5281/zenodo.3893991 (2020).

Acknowledgements We thank the patients and families who donated tissue to this study; M. Madden and M. Korrer for assistance with sample acquisition; members of the J.M.B. laboratory and B. I. Reinfeld for their constructive input; and E. J. Philips, S. Mallal, P. Steinberger and J. Sidney for cell lines and reagents. This work was supported by F30CA236157, T32GM007347 (to M.L.A.), T32DK007061 (to J.J.W.), R01HL141466 (to J.J.M.), R01HL155990 (to J.J.M.), R01CA227481 (to D.B.J. and J.M.B.), R01HL156021 (to J.M.B. and J.J.M.), P30 AI110527 (to S.M.), Susan and Luke Simons Directorship in Melanoma, Van Stephenson Melanoma Research Fund, and James C. Bradford Melanoma Fund (to D.B.J). K.A. is supported by an American Heart Association Career Development Award (929347). W.C.M. is supported by the Mandema-Stipendium of the Junior Scientific Masterclass 2020-10 of the University Medical Center Groningen and by the Dutch Heart Foundation (Dekker grant 03-005-2021-T005). S.Z. is supported by National Natural Science Foundation of China (82100677). E.J.P. receives funding from the National Institutes of Health R01HG010863, R01AI152183 U01AI154659) and from the National Health and Medical Research Council of Australia. J.P.A. is a CPRIT Distinguished Scholar in Cancer Research. We acknowledge the Translational Pathology Shared Resource supported by NCI/NIH Cancer Center Support grant P30CA068485 and the Shared Instrumentation grant S10 OD023475-01A1 for the Leica Bond RX. Staff at The Vanderbilt VANTAGE Core, including A. Jones and L. Raju, provided technical assistance for this work. VANTAGE is supported in part by a CTSA grant (UL1TR002243), the Vanderbilt Ingram Cancer Center (P30 CA68485), the Vanderbilt Vision Center (P30 EY08126), the NIH/NCRR (G20 RR030956), and an NIH High-End Equipment Grant (S10OD025092). Figs. 1a and 4b were created with BioRender.com.

Author contributions M.L.A., J.J.M. and J.M.B. conceived and designed the study and drafted the manuscript. W.C.M., E.M.S., E.T., J.Q., S.Z. and Y.Z. managed the mouse colony and identified appropriate mice for each experiment. M.L.A., W.C.M., E.M.S., M.G.C., X.S., J.J.W., E.T., J.Q., A.H. and A.L.T. performed mouse necropsies, tissue dissociation and cryopreservation. M.L.A. performed scRNA–TCR-seq and bulk TCR-seq data analyses and figure generation. M.L.A., A.L.T. and X.S. prepared samples for single-cell sequencing. W.C.M. and E.M.S. performed antibody-mediated depletion studies. A.S. provided expertise and performed tail vein injections for adoptive transfer studies. M.L.A. and M.G.C. performed antigen discovery, epitope identification and MHC blocking experiments. B.C.T. performed quantitative PCR. W.T. performed the dexamethasone treatment study. S.C.W. and J.P.A. provided expertise regarding the mouse model and myocarditis phenotype. S.R.O. provided technical expertise in experimental design and manuscript editing. J.C.R. provided immunology expertise. P.B.F. provided expertise regarding single-cell studies. E.J.P. and S.M. provided expertise in experimental design regarding LCLs, antigen discovery and MHC blockade. K.A. provided expertise in cardiac pathology from non-myocarditis phenotypes. D.B.J. and J.J.M. provided clinical expertise, assistance in acquiring human samples for this study and assistance with manuscript writing. M.L.A. analysed all data generated in this study. J.J.M. and J.M.B. obtained funding for this study.

Competing interests M.L.A. is listed as a co-inventor on a provisional patent application for methods to predict therapeutic outcomes using blood-based gene expression patterns, which is owned by Vanderbilt University Medical Center, and is currently unlicensed. S.C.W. is currently an employee of, and has ownership interest in, Spotlight Therapeutics. S.C.W. has received personal fees from BioEntre and AlphaSights. S.C.W. is an inventor on a patent related to a genetic mouse model of immune checkpoint blockade induced immune-related adverse events (PCT/US2019/050551) pending to the Board of Regents, The University of Texas System and patent applications submitted by Spotlight Therapeutics related to in vivo gene editing. K.A. serves on the Data Safety Monitoring Board for ACI Clinical. J.C.R. is a founder, scientific advisory board member and stockholder of Sitryx Therapeutics, a scientific advisory board member and stockholder of Caribou Biosciences, a member of the scientific advisory board of Nirogy Therapeutics, has consulted for Merck, Pfizer and Mitobridge within the past 3 years, and has received research support from Incyte, Calithera Biosciences and Tempest Therapeutics. P.B.F. receives research support from Incyte. D.B.J. has served on advisory boards or as a consultant for BMS, Catalyst Biopharma, Iovance, Jansen, Mallinckrodt, Merck, Mosaic ImmunoEngineering, Novartis, Oncosec, Pfizer and Targovax, has received research funding from BMS and Incyte, and has patents pending for use of MHC-II as a biomarker for ICI response, and abatacept as treatment for irAEs. J.P.A. reports personal fees from Achelois, Adaptive Biotechnologies, Apricity Health, BioAtla, Candel Therapeutics, Codiak BioSciences, Dragonfly Therapeutics, Earli, Enable Medicine, Hummingbird, ImaginAb, Jounce Therapeutics, Lava Therapeutics, Lytix Biopharma, Marker Therapeutics, PBM Capital, Phenomic AI, BioNTech, Polaris Pharma, Time Bioventures, Trained Therapeutics, Two Bear Capital, and Venn Biosciences outside the submitted work. In addition, J.P.A. has a patent for a genetic mouse model of immune-checkpoint-blockade-induced irAEs pending to The University of Texas MD Anderson Cancer Center and has received royalties from intellectual property licensed to BMS and Merck. J.J.M. has served on advisory boards for Bristol Myers Squibb, Takeda, Audentes, Deciphera, Janssen, Immuno-Core, Boston Biomedical, Amgen, Myovant, Kurome Therapeutics, Star Therapeutics, ProtinQure, Pharmacyclics, Pfizer, Mallinckrodt Pharmaceuticals, Silverback Therapeutics, Cytokinetics, and AstraZeneca. J.M.B. receives research support from Genentech/Roche, and Incyte, and is an inventor on provisional patents regarding immunotherapy targets and biomarkers in cancer.
No disclosures are reported by the other authors.

Additional information
Supplementary information The online version contains supplementary material available at https://doi.org/10.1038/s41586-022-05432-3.
Correspondence and requests for materials should be addressed to Javid J. Moslehi or Justin M. Balko.
Peer review information *Nature* thanks the anonymous reviewers for their contribution to the peer review of this work. Peer reviewer reports are available.

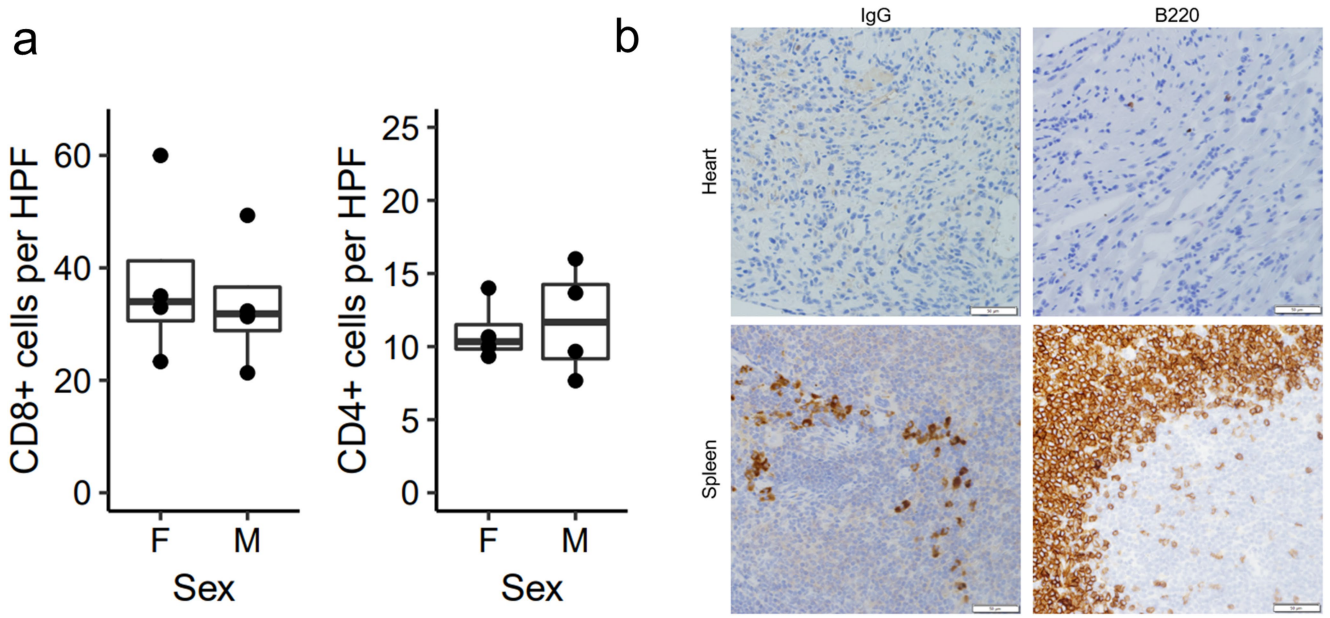

Extended Data Fig. 1 | Myocardial immune infiltrate does not differ by sex. a) Quantification of immunohistochemistry (IHC) for CD8 and CD4 in male and female *Pdcd1*$^{-/-}$ *Ctla4*$^{+/-}$ mice with MC. Cells are counted as number of positive cells per high power (40x) field (HPF). Each data point represents an average of three high power fields per mouse. n = 4 female mice, n = 4 male mice. Box plots show the median, first and third quartiles. The whiskers extend to the maxima and minima but no further than 1.5 times the inter-quartile range. b) Representative IHC for IgG and B220 (CD45R) in hearts of mice with MC and positive control staining in spleen. Images are representative of n = 8 independent *Pdcd1*$^{-/-}$ *Ctla4*$^{+/-}$ mice with MC (n = 4 male; n = 4 female). Scale bars represent 50 μm.

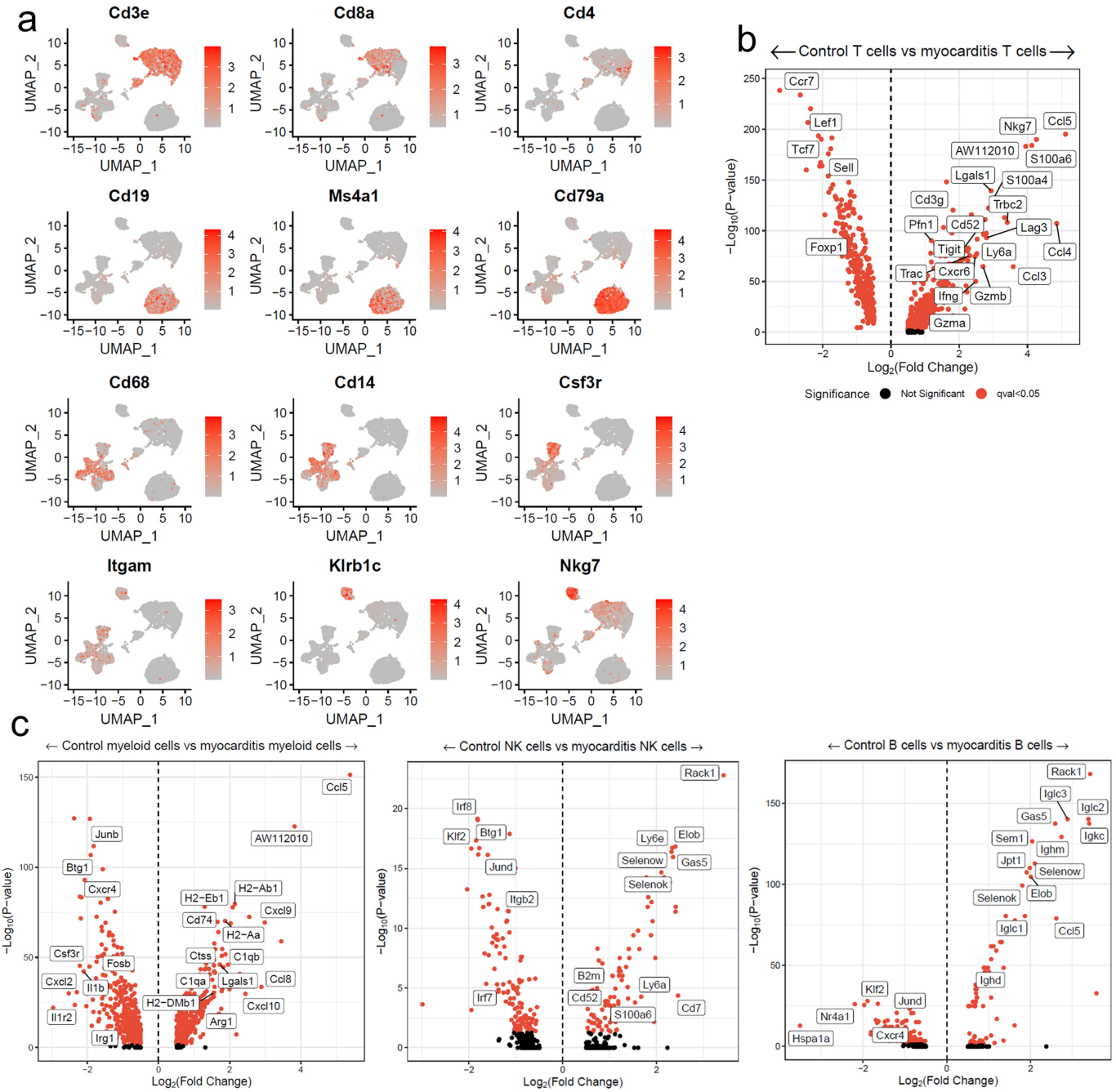

Extended Data Fig. 2 | MC is characterized by activated immune cells and clonal T cells. a) Gene expression of key identity genes, showing cell types of clusters. b) Differential gene expression for T, c) myeloid, B and NK cells in MC compared to control cardiac CD45+ cells. Red indicates FDR-corrected p-value (q-value) < 0.05. Black indicates not significant.

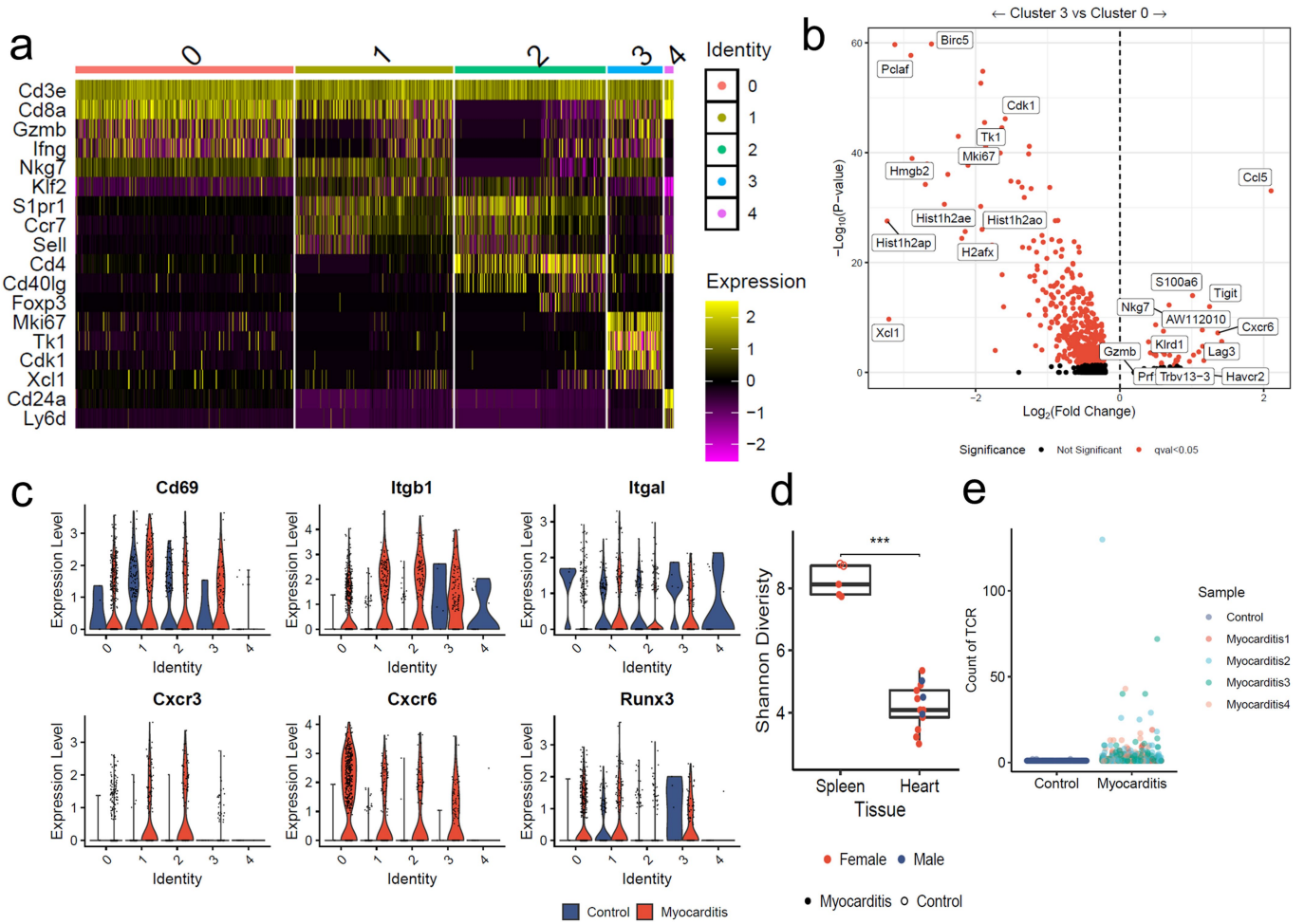

Extended Data Fig. 3 | T cells in MC are effector or proliferating, tissue-resident and clonal. a) Expression of key T cell genes by cluster in single cell data. b) Differential gene expression for Cluster 0 vs. Cluster 3 T cells. Red indicates FDR-corrected p-value (q-value) < 0.05. Black indicates not significant. c) Violin plots show expression of key tissue residency associated genes by cluster and MC vs. control. d) Shannon diversity on bulk TCR sequencing beta chain repertoires. Color indicates sex. Shape indicates whether the tissue was derived from a control wild type mouse (open circle) or a *Pdcd1*$^{-/-}$*Ctla4*$^{+/-}$ mouse with MC (filled circle). P = 0.0002, two-sided Wilcoxon test. Box plots show the median, first and third quartiles. The whiskers extend to the maxima and minima but no further than 1.5 times the inter-quartile range. e) TCR counts in single cell data. MC sample is divided by mouse of origin. Clonal TCRs are found in all 4 sequenced hearts.

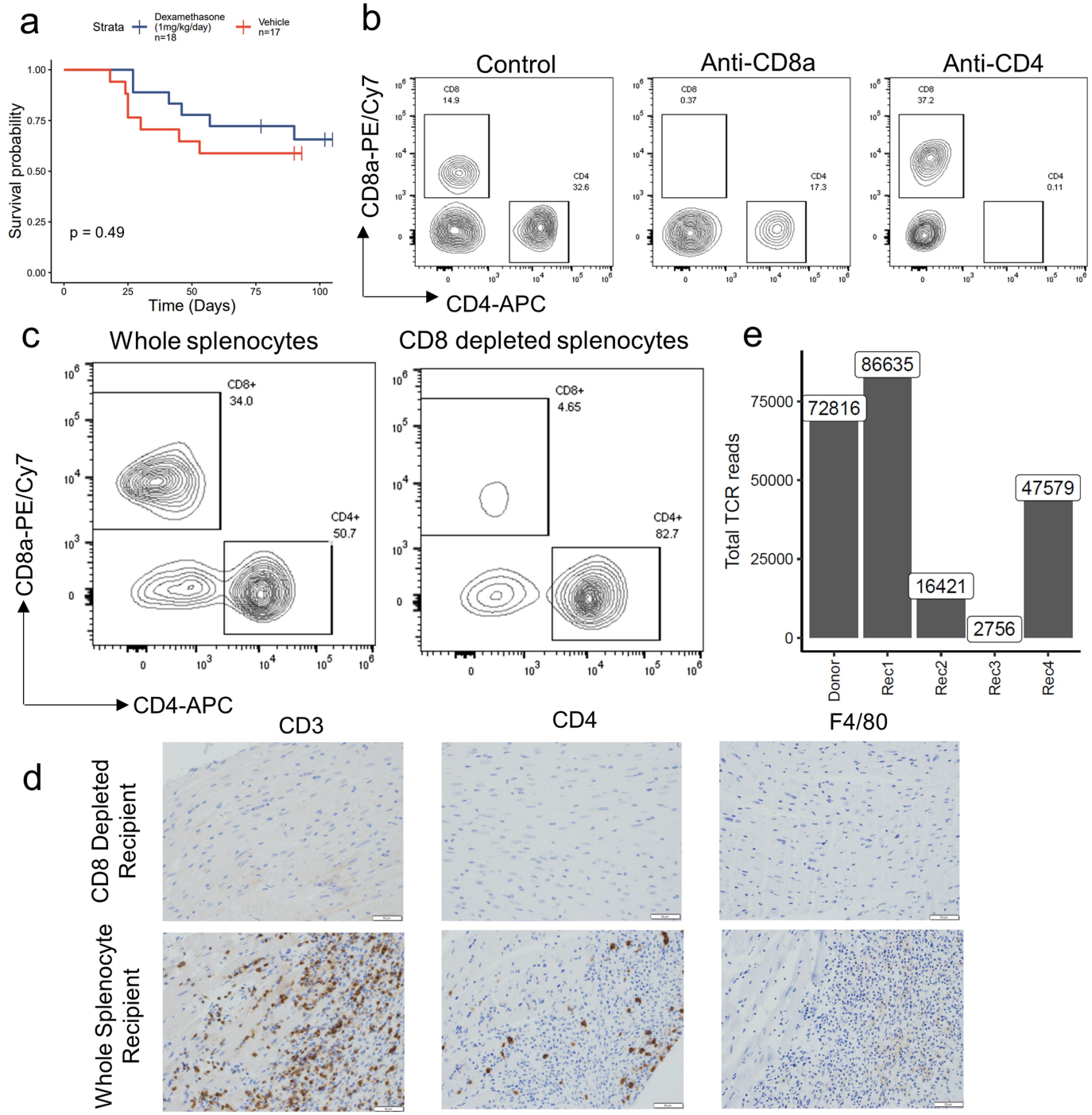

Extended Data Fig. 4 | Confirmation of cell type depletion. a) Female *Pdcd1*$^{-/-}$*Ctla4*$^{+/-}$ mice were treated with dexamethasone (1mg/kg/day; n = 18) or vehicle (n = 17) starting at 21 days of life. Time is measured since birth. P = 0.49, two-sided cox proportional hazard test. b) Representative flow cytometry gated on live CD45+ cells isolated from blood of different treatment groups, at week 3 of treatment. c) Representative flow cytometry on CD8 depleted (via magnetic beads) compared to whole splenocytes used for adoptive transfer. d) Representative immunohistochemistry on hearts of a CD8 depleted splenocyte recipient compared to a whole splenocyte recipient. Only cardiac sections are shown. Scale bars show 50 µm. Representative of n = 10 animals per group. e) Total TCR reads for cardiac TCR beta chain sequencing on donor and recipient hearts.

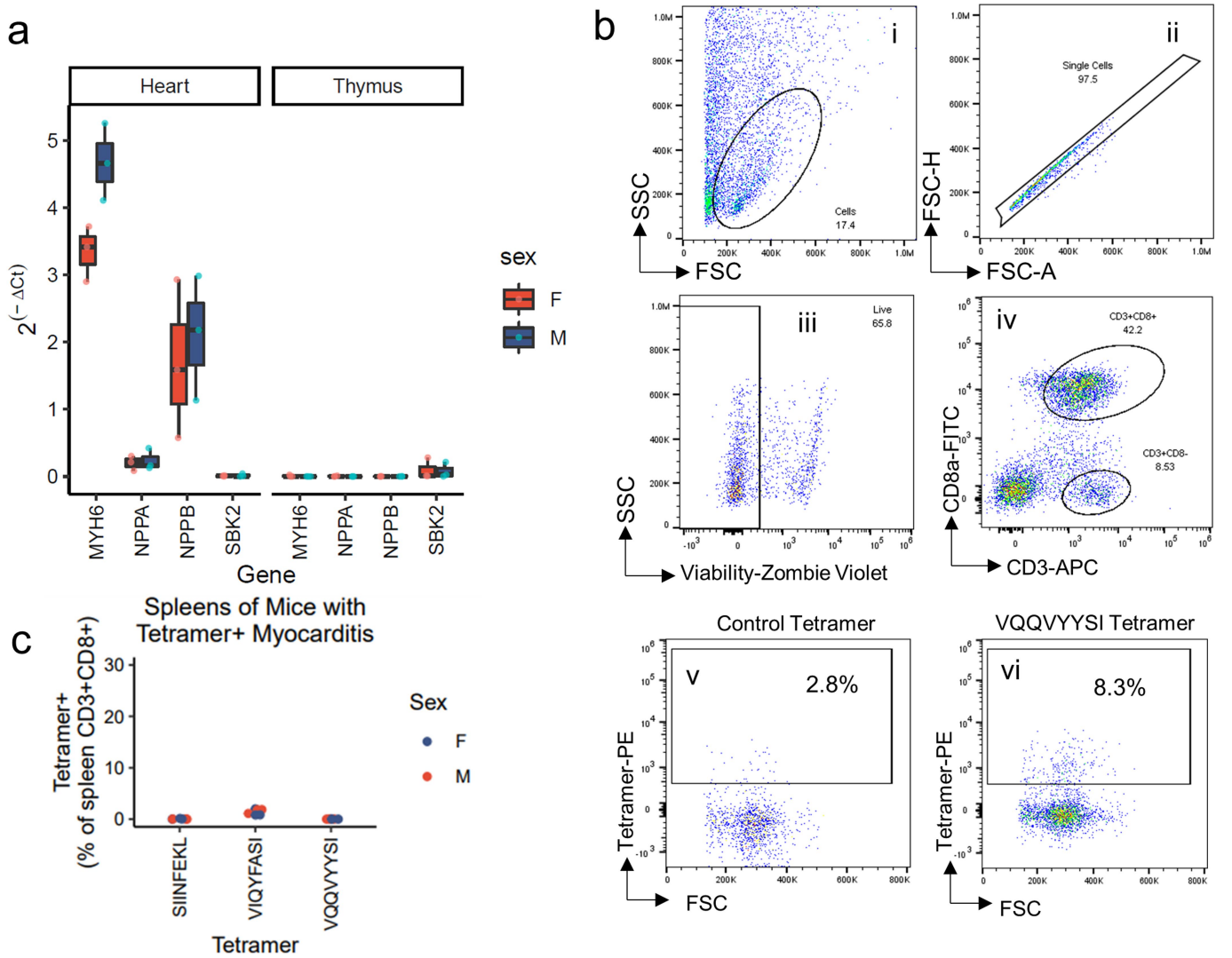

Extended Data Fig. 5 | Thymic expression of Myh6 and flow cytometry gating for murine α-myosin tetramers. a) Gene expression for *Myh6*, *Nppa*, *Nppb*, and *Sbk2* in the heart and thymus of n = 3 each male and female *Pdcd1*$^{-/-}$*Ctla4*$^{+/-}$ mice. Gene expression is normalized to beta-actin. Gene expression is plotted as 2^-(Ct gene of interest minus Ct of beta-actin). Box plots show the median, first and third quartiles. The whiskers extend to the maxima and minima but no further than 1.5 times the inter-quartile range. b) Gating strategy for H2-Kb tetramers on murine heart samples. Debris, doublets and dead cells (Zombie Violet positive) are excluded. CD3+CD8+ cells are used for tetramer analysis. Staining for Control (SIINFEKL) H2-Kb, and VQQVYYSI H2-Kb tetramers are shown. c) Quantification of spleen tetramer positive CD3+CD8+ cells, by sex of the mouse. The spleens used in this experiment correspond to the mice show in Fig. 3f, which all have α-myosin tetramer positive MC.

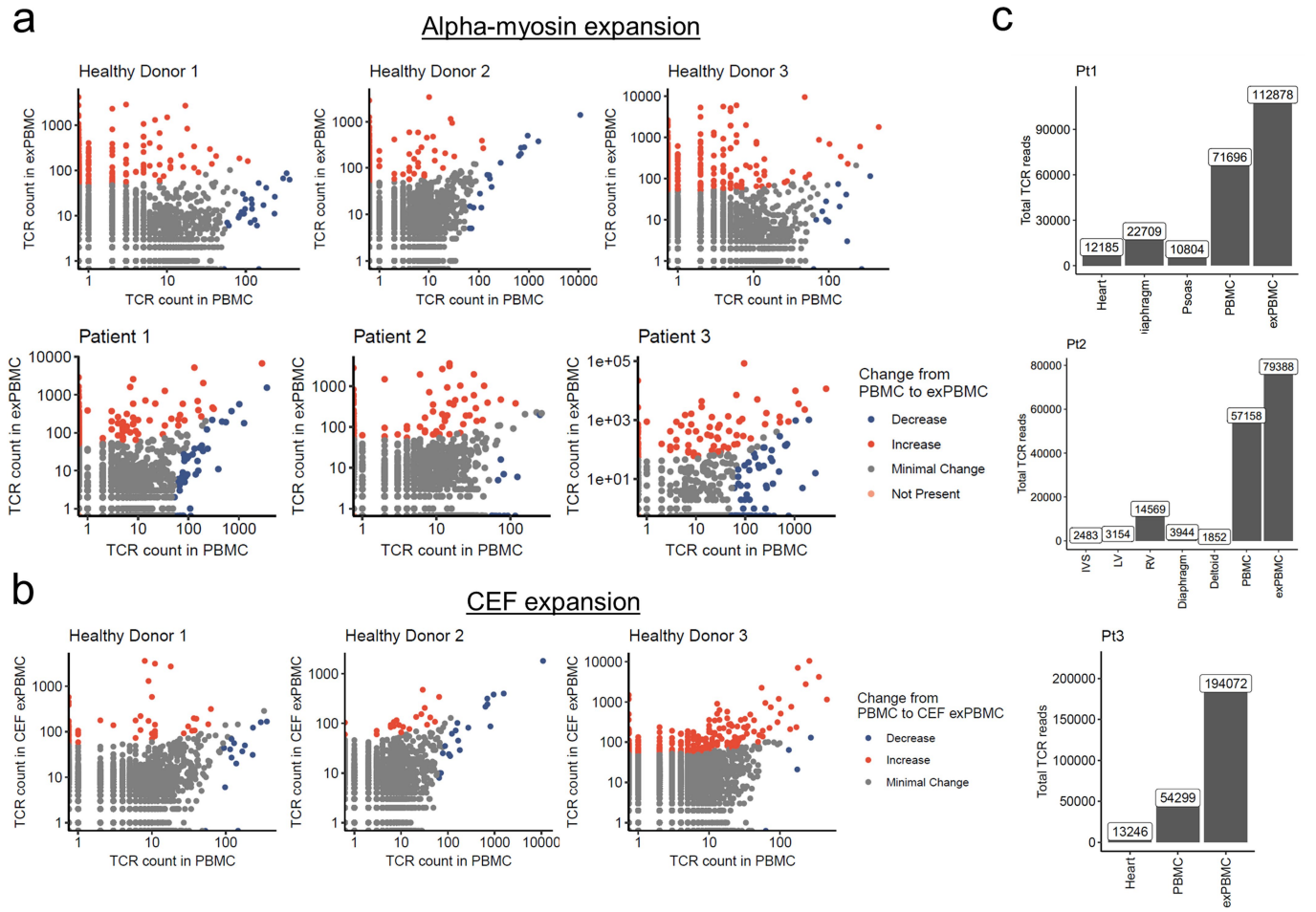

Extended Data Fig. 6 | TCR sequencing on exPBMC shows expansion of α-myosin and CEF specific TCRs. a) Comparison of TCR beta chain abundance in α-myosin exPBMC and pre-expansion PBMC for all patients. Each plot is within the same patient only. Color represents change from PBMC to exPBMC. Minimal change is less than a 50 read count change. b) Comparison of TCR beta chain abundance in CEF exPBMC and pre-expansion PBMC for all healthy donors. Color represents change from PBMC to CEF exPBMC. Minimal change is less than a 50 read count change. c) Total TCR reads for biopsy (heart), autopsy, and PBMC samples from patients 1, 2 and 3.

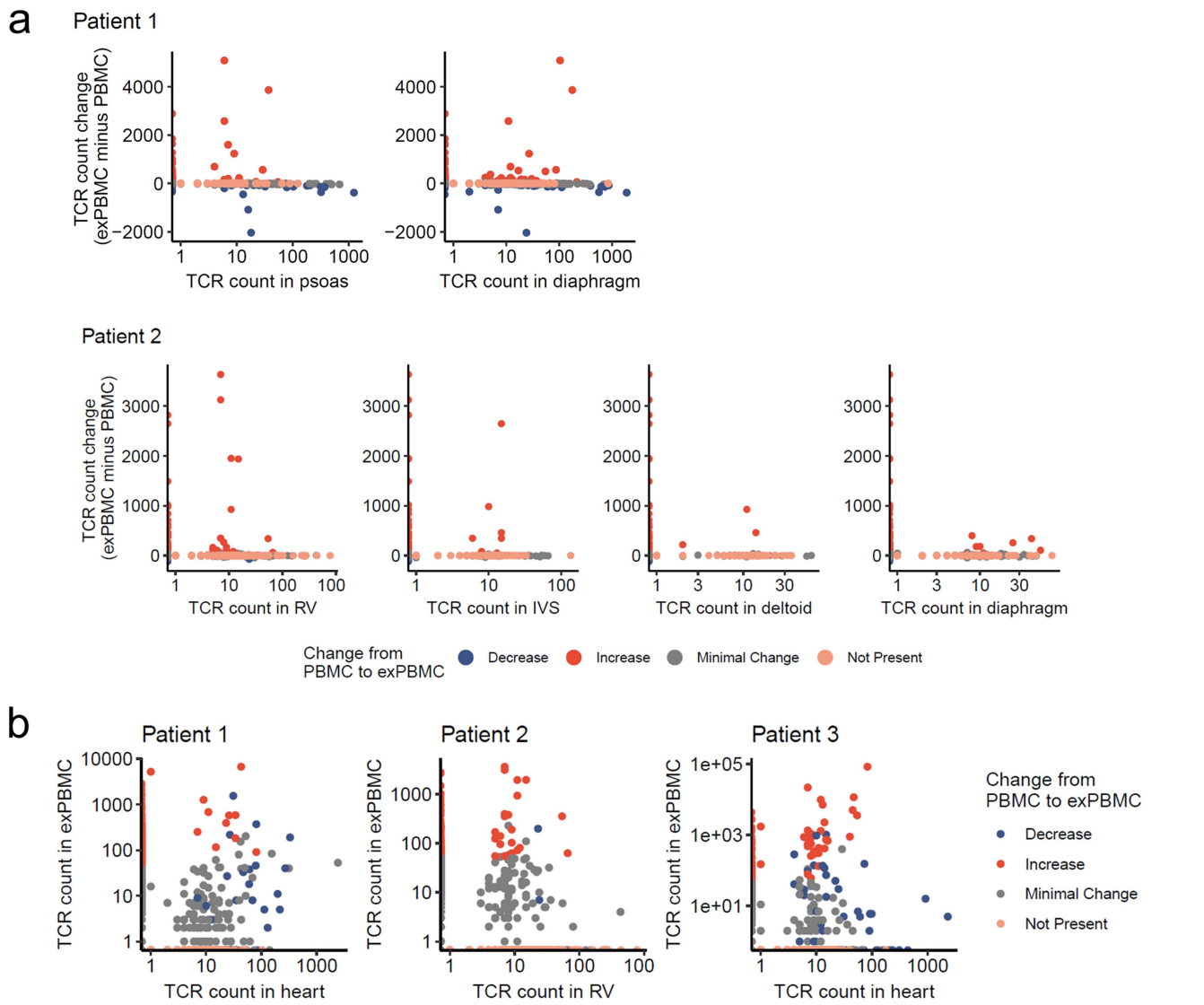

Extended Data Fig. 7 | α-myosin expanded TCRs are found in the hearts and skeletal muscles of patients with ICI-MC. a) Change in TCR counts from PBMC to α-myosin exPBMC plotted by abundance of the same TCR beta chain in the autologous inflamed cardiac or skeletal muscle tissue of each patient. Minimal change is less than a 50 read count change. Not present means not found in either PBMC or exPBMC, but present in indicated tissue. b) Comparison of TCR beta chain abundance in α-myosin exPBMC and heart (biopsy for patient 1 and 3 or right ventricle for patient 2). Color represents change from PBMC to exPBMC. Minimal change is less than a 50 read count change. Not present means not found in either PBMC or exPBMC, but present in heart.

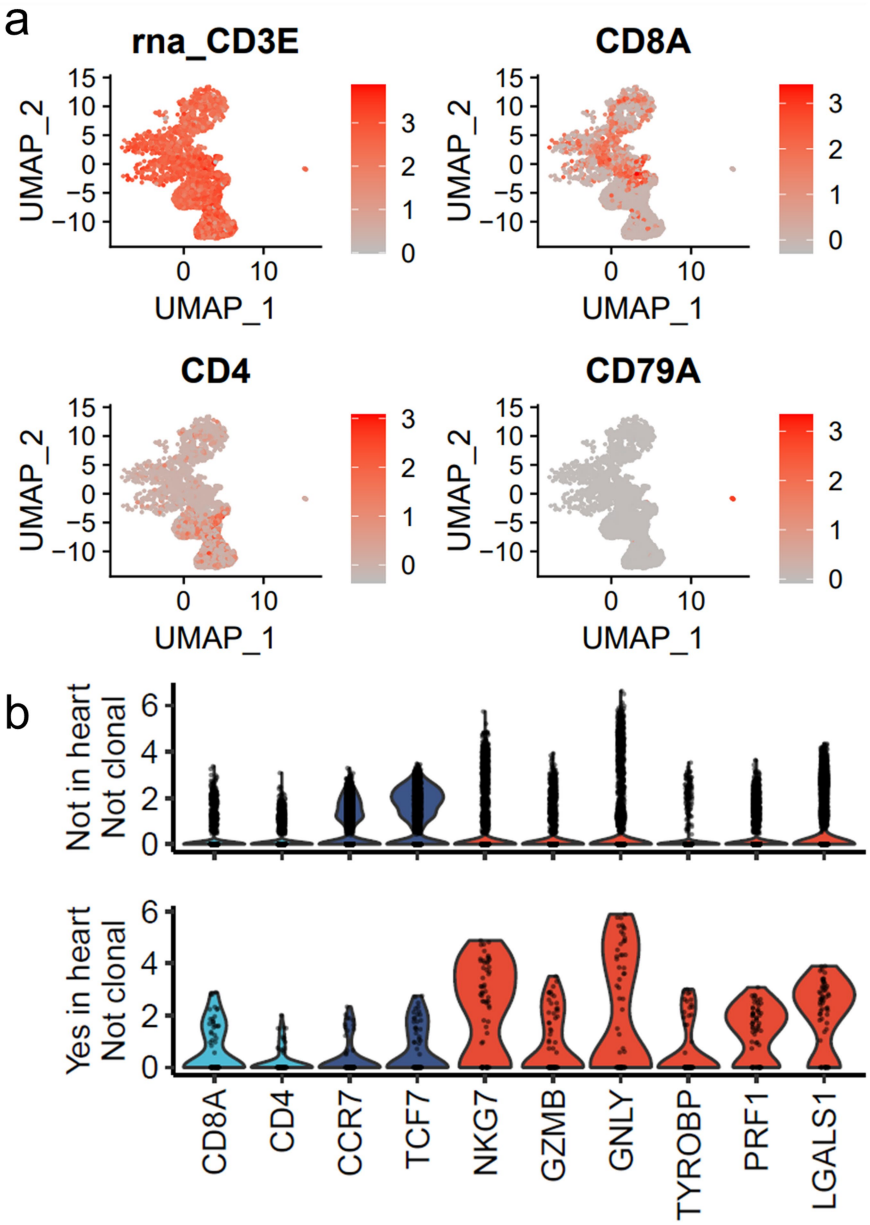

Extended Data Fig. 8 | Purity analysis for single cell sequencing on exPBMCs from patient 1. a) Gene expression is shown on single cell sequencing of CD3 sorted exPBMCs from patient 1. b) Violin plots of key gene expression by presence or absence in cardiac TCR repertoire and clonality in exPBMC. Identity genes are shown in light blue. Genes associated with naïve T cells are shown in dark blue. Genes associated with T cell activation are shown in red.

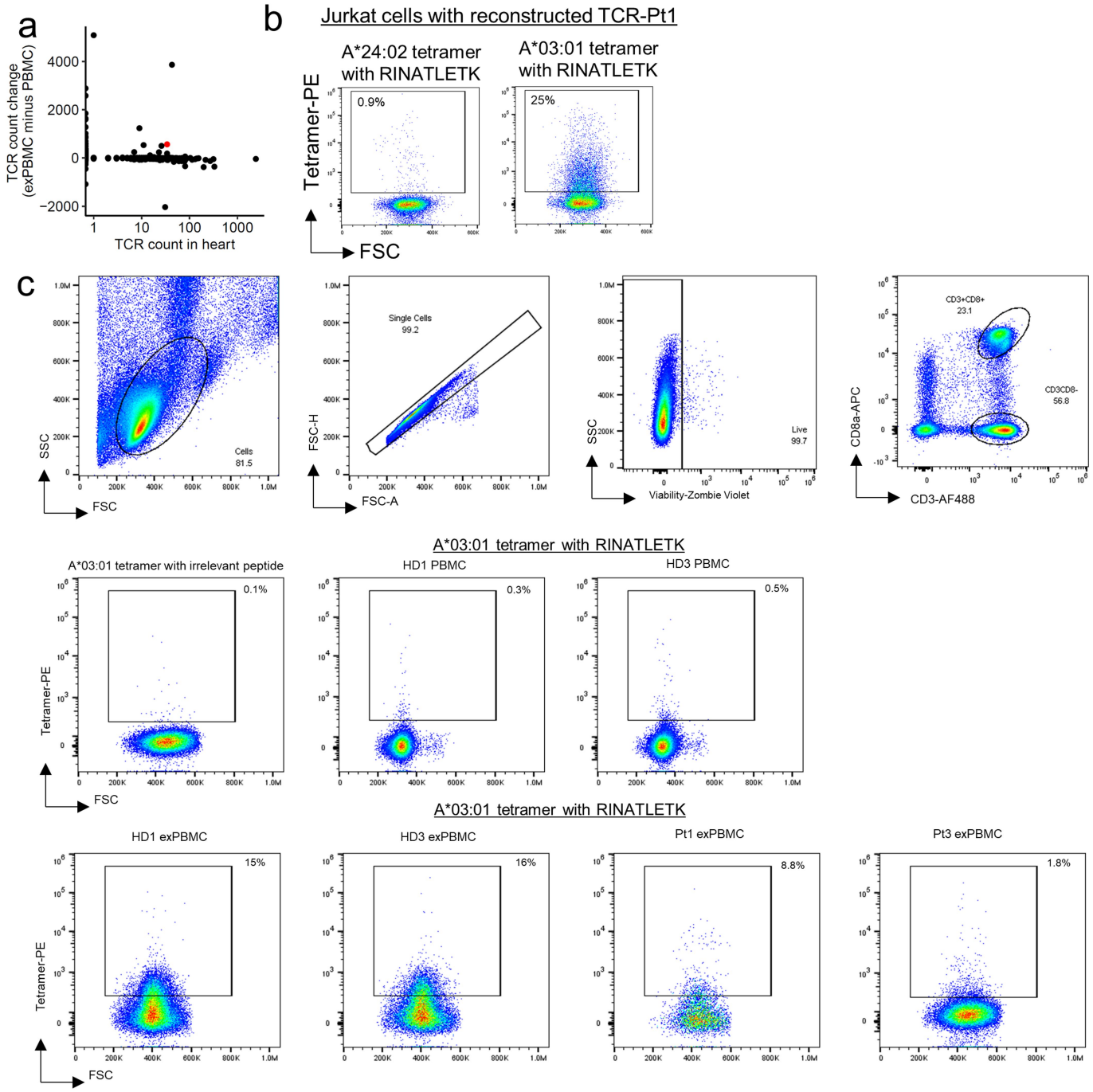

Extended Data Fig. 9 | TCR from Pt 1 exPBMC recognizes α-myosin epitope. a) TCR-Pt1, which was cloned and transduced into Jurkat NFAT-GFP reporter cells, is shown in red on the same plot show in Fig. 4c. This shows the expansion of this TCR in the exPBMC and abundance in the heart. b) Representative flow cytometry scatter plots are shown for the TCR-pt1 Jurkat cell line is stained with A*24:02 tetramer with RINATLETK or A*03:01 tetramer with RINATLETK. c) Full flow cytometry gating strategy for human PBMC and exPBMC tetramer staining. Debris, doublets and dead cells (Zombie Violet positive) are excluded. CD3+CD8+ cells are used for tetramer analysis. Tetramer staining for all samples is shown.

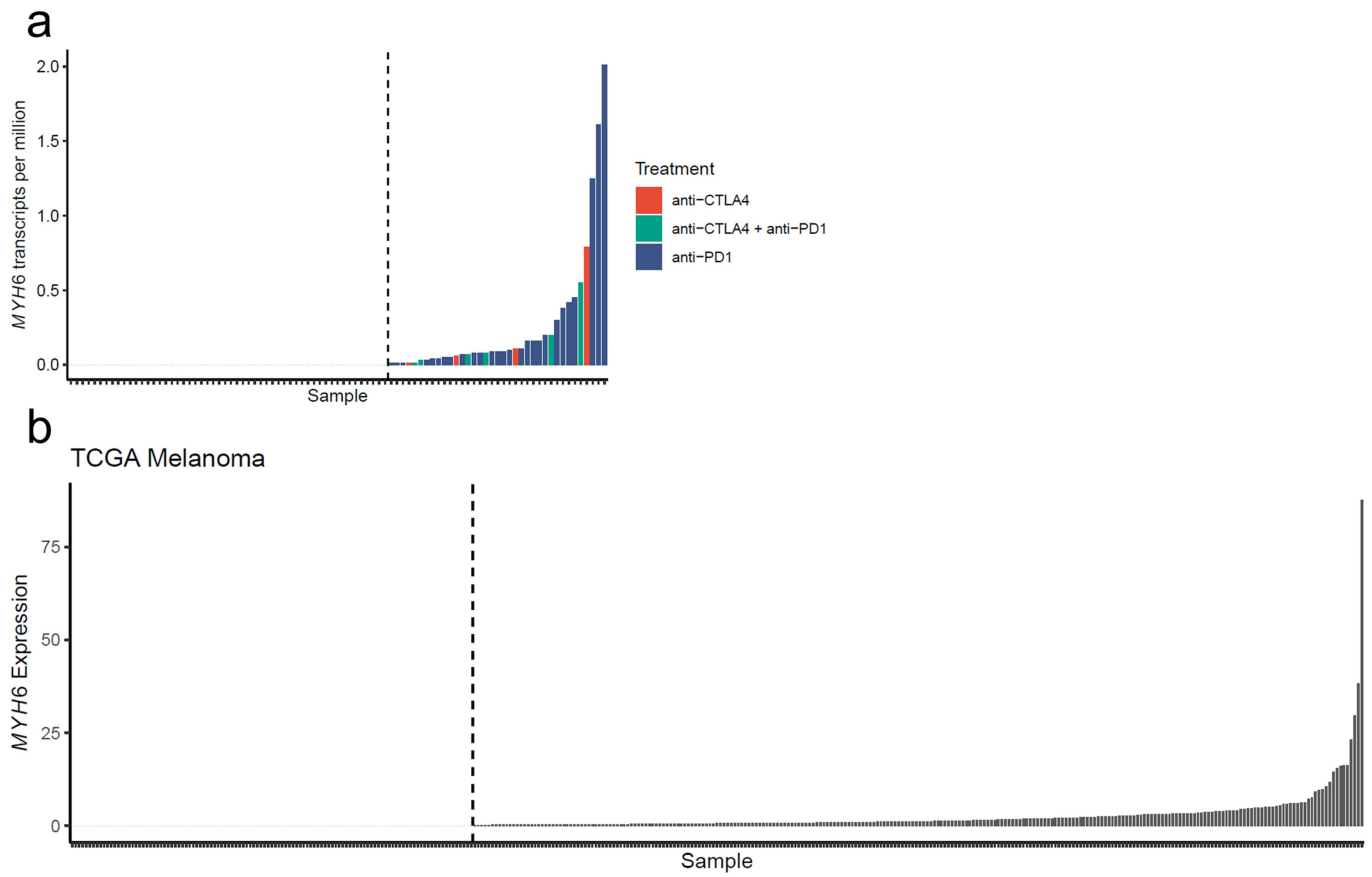

Extended Data Fig. 10 | Tumor-specific MYH6 expression. a) *MYH6* transcripts per million are shown for n = 91 pre-treatment RNA-sequencing melanoma samples. Bars are colored by what ICI treatment the patient received. b) *MYH6* expression is shown for n = 363 melanoma samples accessed from TCGA. Samples to the right of the dotted lines have detectable *MYH6* expression.

Extended Data Table 1 | Amino acid sequences for α-myosin, ANP, BNP and SBK2 peptides included in the peptide library

Name	Sequence	Protein	Name	Sequence	Protein	Name	Sequence	Protein
peptide_1	MTDAQMADFGAAAQYLRKSE	Alpha-myosin	peptide_64	EDECSELKKDIDDLELTLAK	Alpha-myosin	peptide_124	ERRIKELTYQTEEDKKNLMR	Alpha-myosin
peptide_2	LRKSEKERLEAQTRPFDIRT	Alpha-myosin	peptide_65	LTLAKVEKEKHATENKVKNL	Alpha-myosin	peptide_125	KNLMRLQDLVDKLQLKVKAY	Alpha-myosin
peptide_3	FDIRTECFVPDDKEEYVKAK	Alpha-myosin	peptide_66	KVKNLTEEMAGLDEIIAKLT	Alpha-myosin	peptide_126	KVKAYKRQAEEAEEQANTNL	Alpha-myosin
peptide_4	YVKAKVVSREGGKVTAETEN	Alpha-myosin	peptide_67	IAKLTKEKKALQEAHQQALD	Alpha-myosin	peptide_127	ANTNLSKFRKVQHELDEAEE	Alpha-myosin
peptide_5	AETENGKTVTIKEDQVMQQN	Alpha-myosin	peptide_68	QQALDDLQAEEDKVNTLTKS	Alpha-myosin	peptide_128	DEAEERADIAESQVNKLRAK	Alpha-myosin
peptide_6	VMQQNPPKFDKIEDMAMLTF	Alpha-myosin	peptide_69	TLTKSKVKLEQQVDDLEGSL	Alpha-myosin	peptide_129	KLRAKSRDIGAKKMHDEE	Alpha-myosin
peptide_7	AMLTFLHEPAVLYNLKERYA	Alpha-myosin	peptide_70	LEGSLEQEKKVRMDLERAKR	Alpha-myosin	19A	KSRVIFQLKA	Alpha-myosin
peptide_9	FCVTVNPYKWLPVYNAEVVA	Alpha-myosin	peptide_71	ERAKRKLEGDLKLTQESIMD	Alpha-myosin	19B	FQLKAERNYH	Alpha-myosin
peptide_10	AEVVAAYRGKKRSEAPPHIF	Alpha-myosin	peptide_72	ESIMDLENDKLQLEEKLKKK	Alpha-myosin	19C	ERNYHIFYQI	Alpha-myosin
peptide_11	PPHIFSISDNAYQYMLTDRE	Alpha-myosin	peptide_73	KLKKKEFDISQQNSKIEDEQ	Alpha-myosin	55A	DALLVIQWNI	Alpha-myosin
peptide_12	LTDRENQSILITGESGAGKT	Alpha-myosin	peptide_74	IEDEQALALQLQKKLKENQA	Alpha-myosin	55B	IQWNIRAFMG	Alpha-myosin
peptide_13	GAGKTVNTKRVIQYFASIAA	Alpha-myosin	peptide_75	KENQARIEELEEELEAERTA	Alpha-myosin	55C	RAFMGVKNWP	Alpha-myosin
peptide_14	ASIAAIGDRSKKENPNANKG	Alpha-myosin	peptide_76	AERTARAKVEKLRSDLSREL	Alpha-myosin	SBK2_1	MPGKQSEDKPMEVSTVEDGG	SBK2
peptide_15	NANKGTLEDQIIQANPALEA	Alpha-myosin	peptide_77	LSRELEEISERLEEAGGATS	Alpha-myosin	SBK2_2	VEDGGDEGLGGLTVEELQQG	SBK2
peptide_16	PALEAFGNAKTVRNDNSSRF	Alpha-myosin	peptide_78	GGATSVQIEMNKKREAEFQK	Alpha-myosin	SBK2_3	ELQQGQEAALALEDMMALSA	SBK2
peptide_17	NSSRFGKFIRIHFGATGKLA	Alpha-myosin	peptide_79	AEFQKMRRDLEEATLQHEAT	Alpha-myosin	SBK2_4	MALSAQTLVQTEVEELYEEV	SBK2
peptide_18	TGKLASADIETYLLEKSRVI	Alpha-myosin	peptide_80	QHEATAAALRKKHADSVAEL	Alpha-myosin	SBK2_5	LYEEVRPLGQGRFGRVLLVT	SBK2
peptide_20	IFYQILSNKKPELLDMLLVT	Alpha-myosin	peptide_81	SVAELGEQIDNLQRVKQKLE	Alpha-myosin	SBK2_6	VLLVTHRQKGTPLALKQLPK	SBK2
peptide_21	MLLVTNNPYDYAFVSQGEVS	Alpha-myosin	peptide_82	KQKLEKEKSEFKLELDDVTS	Alpha-myosin	SBK2_7	KQLPKQSTSLRGFLYEFCVG	SBK2
peptide_23	LATDSAFDVLSFTAEEKAGV	Alpha-myosin	peptide_83	DDVTSNMEQIIKAKANLEKV	Alpha-myosin	SBK2_8	EFCVGLSLGTHSAIVTAYGI	SBK2
peptide_24	EKAGVYKLTGAIMHYGNMKF	Alpha-myosin	peptide_84	NLEKVSRTLEDQANEYRVKL	Alpha-myosin	SBK2_9	TAYGIGIESANSYSFLTEPV	SBK2
peptide_25	GNMKFKQKQREEQAEPDGTE	Alpha-myosin	peptide_85	YRVKLEEAQRSLNDFTTQRA	Alpha-myosin	SBK2_10	LTEPVLHGDLITFIQPKVGL	SBK2
peptide_26	PDGTEDADKSAYLMGLNSAD	Alpha-myosin	peptide_86	TTQRAKLQTENGELARQLEE	Alpha-myosin	SBK2_11	PKVGLPQPAAQRCAAQLASA	SBK2
peptide_27	LNSADLLKGLCHPRVKVGNE	Alpha-myosin	peptide_87	RQLEEKEALISQLTRGKLSY	Alpha-myosin	SBK2_12	QLASALEHIHSHGLVYRDLK	SBK2
peptide_28	KVGNEYVTKGQSVQQVYYSI	Alpha-myosin	peptide_88	GKLSYTQQMEDLKRQLEEEG	Alpha-myosin	SBK2_13	YRDLKPENVLVCDPACQRVK	SBK2
peptide_29	VYYSIGALAKSVYEKMFNWM	Alpha-myosin	peptide_89	LEEEGKAKNALAHALQSSRH	Alpha-myosin	SBK2_14	CQRVKLTDFGHTRPRGTLLR	SBK2
peptide_30	MFNWMVTRINATLETKQPRQ	Alpha-myosin	peptide_90	QSSRHDCDLLREQYEEEMEA	Alpha-myosin	SBK2_15	GTLLRLTGPPIPYTAPELCA	SBK2
peptide_31	KQPRQYFIGVLDIAGFEIFD	Alpha-myosin	peptide_91	EEMEAKAELQRVLSKANSEV	Alpha-myosin	SBK2_16	PELCAPPPLPEGLPIQPSLD	SBK2
peptide_32	FEIFDFNSFEQLCINFTNEK	Alpha-myosin	peptide_92	ANSEVAQWRTKYETDAIQRT	Alpha-myosin	SBK2_17	QPSLDAWALGVLIFCLLTGY	SBK2
peptide_33	FTNEKLQQFFNHHMFVLEQE	Alpha-myosin	peptide_93	AIQRTEELEEAKKKLAQRLQ	Alpha-myosin	SBK2_18	LLTGYFPWDQPLVEVDPFFE	SBK2
peptide_34	VLEQEEYKKEGIEWEFIDFG	Alpha-myosin	peptide_94	AQRLQDAEEAVEAVNAKCSS	Alpha-myosin	SBK2_19	DPFFEDFLIWQASGQPQDRP	SBK2
peptide_35	FIDFGMDLQACIDLIEKPMG	Alpha-myosin	peptide_95	AKCSSLEKTKHRLQNEIEDL	Alpha-myosin	SBK2_20	PQDRPQPWYSLSPAADTLLW	SBK2
peptide_36	EKPMGIMSILEEECMFPKAS	Alpha-myosin	peptide_96	EIEDLMVDVERSNAAAAALD	Alpha-myosin	SBK2_21	DTLLWGLLDPHPRKRNPVGS	SBK2
peptide_37	FPKASDMTFKAKLYDNHLGK	Alpha-myosin	peptide_97	AAALDKKQRNFDKILAEWKQ	Alpha-myosin	SBK2_22	NPVGSIKSYLGQPWKQREGE	SBK2
peptide_38	NHLGKSNNFQKPRNVKGKQE	Alpha-myosin	peptide_98	AEWKQKYEESQSELESSQKE	Alpha-myosin	SBK2_23	QREGEAEELATELREDGWRG	SBK2
peptide_39	KGKQEAHFSLVHYAGTVDYN	Alpha-myosin	peptide_99	SSQKEARSLSTELFKLKNAY	Alpha-myosin	SBK2_24	DGWRGGQEAAKGEQPAC	SBK2
peptide_40	TVDYNIMGWLEKNKDPLNET	Alpha-myosin	peptide_100	LKNAYEESLEHLETFKRENK	Alpha-myosin	NPPA_26	FWLPGHIGANPVYSAVSNTD	ANP
peptide_41	PLNETVVGLYQKSSLKLMAT	Alpha-myosin	peptide_101	KRENKNLQEEISDLTEQLGE	Alpha-myosin	NPPA_27	VSNTDLMDFKNLLDHLEEKM	ANP
peptide_42	KLMATLFSTYASADTGDSGK	Alpha-myosin	peptide_102	EQLGEGGKNVHELEKIRKQL	Alpha-myosin	NPPA_28	LEEKMPVEDEVMPPQALSEQ	ANP
peptide_43	GDSGKGKGGKKKGSSFQTVS	Alpha-myosin	peptide_103	IRKQLEVEKLELQSALEEAE	Alpha-myosin	NPPA_29	ALSEQTEEAGAALSSLPEVP	ANP
peptide_44	FQTVSALHRENLNKLMTNLK	Alpha-myosin	peptide_104	LEEAEASLEHEEGKILRAQL	Alpha-myosin	NPPA_30	LPEVPPWTGEVNPPLRDGSA	ANP
peptide_45	MTNLKTTHPHFVRCIIPNER	Alpha-myosin	peptide_105	LRAQLEFNQIKAEIERKLAE	Alpha-myosin	NPPA_31	RDGSALGRSPWDPSDRSALL	ANP
peptide_46	IPNERKAPGVMDNPLVMHQL	Alpha-myosin	peptide_106	RKLAEKDEEMEQAKRNHLRM	Alpha-myosin	NPPA_32	RSALLKSKLRALLAGPRSLR	ANP
peptide_47	VMHQLRCNGVLEGIRICRKG	Alpha-myosin	peptide_108	ETRSRNEALRVKKKMEGDLN	Alpha-myosin	NPPA_33	PRSLRRSSCFGGRIDRIGAQ	ANP
peptide_48	ICRKGFPNRILYGDFRQRYR	Alpha-myosin	peptide_109	EGDLNEMEIQLSQANRIASE	Alpha-myosin	NPPA_34	RIGAQSGLGCNSFRYRR	ANP
peptide_49	RQRYRILNPAAIPEGQFIDS	Alpha-myosin	peptide_110	RIASEAQKHLKNSQAHLKDT	Alpha-myosin	BNP_35	MDLLKVLSQMILFLLFLYLS	BNP
peptide_50	QFIDSRKGAEKLLGSLDIDH	Alpha-myosin	peptide_111	HLKDTQLQLDDAVHANDDLK	Alpha-myosin	BNP_36	FLYLSPLGGHSYPLGSPSQS	BNP
peptide_51	LDIDHNQYKFGHTKVFFKAG	Alpha-myosin	peptide_112	NDDLKENIAIVERRNNLLQA	Alpha-myosin	BNP_37	SPSQSPEQFKMQKLLELIRE	BNP
peptide_52	FFKAGLLGLLEEMRDERLSR	Alpha-myosin	peptide_113	NLLQAELEELRAVVEQTERS	Alpha-myosin	BNP_38	ELIREKSEEMAQRQLLKDQG	BNP
peptide_53	ERLSRIITRIQAQARGQLMR	Alpha-myosin	peptide_114	QTERSRKLAEQELIETSERV	Alpha-myosin	BNP_39	LKDQGLTKEHPKRVLRSQGS	BNP
peptide_54	GQLMRIEFKKIVERRDALLV	Alpha-myosin	peptide_115	TSERVQLLHSQNTSLINQKK	Alpha-myosin	BNP_40	RSQGSTLRVQQRPQNSKVTH	BNP
peptide_56	VKNWPWMKLYFKIKPLLKSA	Alpha-myosin	peptide_116	INQKKKMESDLTQLQTEVEE	Alpha-myosin	BNP_41	SKVTHISSCFGHKIDRIGSV	BNP
peptide_57	LLKSAETEKEMANMKEEFGR	Alpha-myosin	peptide_117	TEVEEAVQECRNAEEKAKKA	Alpha-myosin	BNP_42	RIGSVSRLGCNALKLL	BNP
peptide_58	EEFGRVKDALEKSEARRKEL	Alpha-myosin	peptide_118	KAKKAITDAAMMAEELKKEQ	Alpha-myosin			
peptide_59	RRKELEEKMVSLLQEKNDLQ	Alpha-myosin	peptide_119	LKKEQDTSAHLERMKKNMEQ	Alpha-myosin			
peptide_60	KNDLQLQVQAEQDNLNDAEE	Alpha-myosin	peptide_120	KNMEQTIKDLQHRLDEAEQI	Alpha-myosin			
peptide_61	NDAEERCDQLIKNKIQLEAK	Alpha-myosin	peptide_121	EAEQIALKGGKKQLQKLEAR	Alpha-myosin			
peptide_62	QLEAKVKEMTERLEDEEEMN	Alpha-myosin	peptide_122	KLEARVRELENELEAEQKRN	Alpha-myosin			
peptide_63	EEEMNAELTAKKRKLEDECS	Alpha-myosin	peptide_123	EQKRNAESVKGMRKSERRIK	Alpha-myosin			

Extended Data Table 2 | Prediction scores for binding of α-myosin peptides to MHC-I molecules in C57BL/6 mice generated by TepiTool

Seq #	Peptide start	Peptide end	Peptide	Percentile rank	Allele	Seq #	Peptide start	Peptide end	Peptide	Percentile rank	Allele	Seq #	Peptide start	Peptide end	Peptide	Percentile rank	Allele
1	190	198	RVIQYFASI	0.01	H-2-Kb	1	1207	1215	EQIDNLQRV	0.32	H-2-Db	1	816	823	IQWNIRAF	0.62	H-2-Kb
1	113	120	MIYTYSGL	0.01	H-2-Kb	1	834	842	LYFKIKPLL	0.32	H-2-Kb	1	283	291	NYHIFYQIL	0.62	H-2-Kb
1	650	660	SALHRENLNKL	0.02	H-2-Db	1	271	278	KSRVIFQL	0.32	H-2-Kb	1	1379	1388	TDAIQRTEEL	0.64	H-2-Db
1	644	652	SSFQTVSAL	0.03	H-2-Kb	1	545	553	SDMTFKAKL	0.32	H-2-Kb	1	124	131	TVNPYKWL	0.64	H-2-Kb
1	613	621	SSLKLMATL	0.04	H-2-Db	1	1492	1500	ESLEHLETF	0.33	H-2-Db	1	687	695	DNPLVMHQL	0.64	H-2-Kb
1	282	290	RNYHIFYQI	0.04	H-2-Kb	1	384	391	KSAYLMGL	0.33	H-2-Kb	1	768	778	KAGLLGLLEEM	0.66	H-2-Db
1	191	198	VIQYFASI	0.04	H-2-Kb	1	437	444	FNWMVTRI	0.35	H-2-Kb	1	289	299	QILSNKKPELL	0.66	H-2-Db
1	764	771	KVFFKAGL	0.05	H-2-Kb	1	1861	1869	KNLMRLQDL	0.35	H-2-Kb	1	709	717	KGFPNRILY	0.67	H-2-Db
1	824	832	MGVKNWPWM	0.06	H-2-Db	1	1257	1265	QANEYRVKL	0.35	H-2-Kb	1	487	494	QQFFNHHM	0.68	H-2-Db
1	322	330	ASIDDSEEL	0.06	H-2-Db	1	157	165	ISDNAYQYM	0.37	H-2-Kb	1	1643	1652	KHLKNSQAHL	0.68	H-2-Db
1	827	834	KNWPWMKL	0.06	H-2-Kb	1	417	425	SVQQVYYSI	0.37	H-2-Kb	1	599	607	KDPLNETVV	0.69	H-2-Db
1	613	621	SSLKLMATL	0.06	H-2-Kb	1	490	497	FNHHMFVL	0.37	H-2-Kb	1	486	494	LQQFFNHHM	0.69	H-2-Kb
1	1759	1767	KAITDAAMM	0.07	H-2-Db	1	833	841	KLYFKIKPL	0.39	H-2-Kb	1	532	540	MSILEEECM	0.7	H-2-Db
1	644	652	SSFQTVSAL	0.07	H-2-Db	1	123	131	VTVNPYKWL	0.39	H-2-Kb	1	69	77	VTIKEDQVM	0.7	H-2-Db
1	1242	1250	KAKANLEKV	0.07	H-2-Db	1	441	448	VTRINATL	0.39	H-2-Kb	1	1201	1209	SVAELGEQI	0.71	H-2-Db
1	730	738	AAIPEGQFI	0.08	H-2-Db	1	883	891	LQEKNDLQL	0.4	H-2-Db	1	1380	1388	DAIQRTEEL	0.72	H-2-Db
1	684	692	GVMDNPLVM	0.08	H-2-Db	1	1409	1416	VNAKCSSL	0.41	H-2-Kb	1	1488	1497	NAYEESLEHL	0.72	H-2-Db
1	479	486	INFTNEKL	0.08	H-2-Kb	1	261	269	SADIETYLL	0.42	H-2-Db	1	190	198	RVIQYFASI	0.72	H-2-Db
1	909	917	QLIKNKIQL	0.09	H-2-Db	1	1484	1494	FKLKNAYEESL	0.42	H-2-Db	1	1649	1657	QAHLKDTQL	0.72	H-2-Db
1	1893	1901	TNLSKFRKV	0.11	H-2-Kb	1	322	331	ASIDDSEELL	0.43	H-2-Db	1	1723	1732	TSLINQKKKM	0.72	H-2-Kb
1	421	428	VYYSIGAL	0.12	H-2-Kb	1	1239	1247	QIIKAKANL	0.43	H-2-Kb	1	1437	1444	SNAAAAAL	0.72	H-2-Kb
1	356	363	AIMHYGNM	0.12	H-2-Kb	1	79	87	QNPPKFDKI	0.43	H-2-Kb	1	597	607	KNKDPLNETVV	0.73	H-2-Db
1	148	157	SEAPPHIFSI	0.13	H-2-Db	1	649	657	VSALHRENL	0.44	H-2-Db	1	1328	1335	KNALAHAL	0.73	H-2-Kb
1	1890	1898	QANTNLSKF	0.13	H-2-Db	1	607	615	VGLYQKSSL	0.44	H-2-Kb	1	1675	1682	IVERRNNL	0.73	H-2-Kb
1	155	165	FSISDNAYQYM	0.14	H-2-Db	1	467	474	EIFDFNSF	0.44	H-2-Kb	1	1757	1767	AKKAITDAAMM	0.75	H-2-Db
1	279	287	KAERNYHIF	0.14	H-2-Db	1	431	440	SVYEKMFNWM	0.44	H-2-Kb	1	642	649	KGSSFQTV	0.75	H-2-Kb
1	311	319	YAFVSQGEV	0.14	H-2-Db	1	562	570	NNFQKPRNV	0.44	H-2-Kb	1	479	489	INFTNEKLQQF	0.76	H-2-Kb
1	487	495	QQFFNHHMF	0.16	H-2-Db	1	355	363	GAIMHYGNM	0.45	H-2-Db	1	550	558	KAKLYDNHL	0.76	H-2-Kb
1	149	157	EAPPHIFSI	0.17	H-2-Db	1	288	298	YQILSNKKPEL	0.45	H-2-Db	1	1764	1771	AAMMAEEL	0.77	H-2-Db
1	113	121	MIYTYSGLF	0.17	H-2-Kb	1	487	496	QQFFNHHMFV	0.46	H-2-Db	1	645	652	SFQTVSAL	0.78	H-2-Kb
1	243	251	SRFGKFIRI	0.18	H-2-Kb	1	93	101	LTFLHEPAV	0.46	H-2-Kb	1	244	251	RFGKFIRI	0.79	H-2-Kb
1	649	657	VSALHRENL	0.18	H-2-Kb	1	823	832	FMGVKNWPWM	0.47	H-2-Db	1	514	522	FGMDLQACI	0.8	H-2-Db
1	282	291	RNYHIFYQIL	0.18	H-2-Kb	1	1655	1663	TQLQLDDAV	0.47	H-2-Db	1	763	771	TKVFFKAGL	0.8	H-2-Kb
1	724	732	YRILNPAAI	0.19	H-2-Db	1	242	251	SSRFGKFIRI	0.47	H-2-Kb	1	544	553	ASDMTFKAKL	0.8	H-2-Kb
1	487	497	QQFFNHHMFVL	0.2	H-2-Db	1	1258	1265	ANEYRVKL	0.48	H-2-Kb	1	426	436	GALAKSVYEKM	0.81	H-2-Db
1	335	342	SAFDVLSF	0.2	H-2-Kb	1	1240	1247	IIKAKANL	0.48	H-2-Kb	1	1830	1839	AEQKRNAESV	0.82	H-2-Db
1	765	772	VFFKAGLL	0.2	H-2-Kb	1	920	928	KVKEMTERL	0.49	H-2-Kb	1	1562	1570	RAQLEFNQI	0.82	H-2-Db
1	147	157	RSEAPPHIFSI	0.21	H-2-Db	1	1479	1486	LSTELFKL	0.5	H-2-Kb	1	1519	1528	GEGGKNVHEL	0.83	H-2-Db
1	1520	1528	EGGKNVHEL	0.21	H-2-Db	1	614	621	SLKLMATL	0.5	H-2-Kb	1	824	834	MGVKNWPWMKL	0.84	H-2-Db
1	666	674	TTHPHFVRC	0.21	H-2-Kb	1	592	602	MGWLEKNKDPL	0.51	H-2-Db	1	157	165	ISDNAYQYM	0.85	H-2-Db
1	431	439	SVYEKMFNW	0.21	H-2-Kb	1	971	980	HATENKVKNL	0.51	H-2-Db	1	488	495	QFFNHHMF	0.85	H-2-Kb
1	650	657	SALHRENL	0.21	H-2-Kb	1	1783	1792	RMKKNMEQTI	0.51	H-2-Db	1	769	778	AGLLGLLEEM	0.86	H-2-Db
1	1587	1595	QAKRNHLRM	0.22	H-2-Db	1	388	396	LMGLNSADL	0.52	H-2-Db	1	282	290	RNYHIFYQI	0.87	H-2-Db
1	682	692	APGVMDNPLVM	0.22	H-2-Db	1	229	237	EAFGNAKTV	0.52	H-2-Db	1	485	495	KLQQFFNHHMF	0.88	H-2-Db
1	1563	1570	AQLEFNQI	0.22	H-2-Kb	1	594	602	WLEKNKDPL	0.52	H-2-Db	1	1157	1165	GATSVQIEM	0.89	H-2-Db
1	418	425	VQQVYYSI	0.22	H-2-Kb	1	149	157	EAPPHIFSI	0.52	H-2-Kb	1	467	477	EIFDFNSFEQL	0.89	H-2-Kb
1	1674	1682	AIVERRNNL	0.23	H-2-Kb	1	1831	1839	EQKRNAESV	0.53	H-2-Db	1	822	832	AFMGVKNWPWM	0.9	H-2-Db
1	881	891	SLLQEKNDLQL	0.24	H-2-Db	1	156	165	SISDNAYQYM	0.53	H-2-Db	1	332	340	ATDSAFDVL	0.9	H-2-Db
1	681	690	KAPGVMDNPL	0.24	H-2-Db	1	389	397	MGLNSADLL	0.53	H-2-Db	1	469	477	FDFNSFEQL	0.9	H-2-Db
1	260	268	ASADIETYL	0.25	H-2-Db	1	227	237	ALEAFGNAKTV	0.53	H-2-Db	1	428	436	LAKSVYEKM	0.91	H-2-Kb
1	1791	1799	TIKDLQHRL	0.25	H-2-Kb	1	164	174	YMLTDRENQSI	0.54	H-2-Db	1	651	660	ALHRENLNKL	0.92	H-2-Db
1	454	461	RQYFIGVL	0.25	H-2-Kb	1	1223	1230	KSEFKLEL	0.54	H-2-Kb	1	1102	1110	LALQLQKKL	0.94	H-2-Kb
1	1490	1500	YEESLEHLETF	0.26	H-2-Db	1	321	330	VASIDDSEEL	0.56	H-2-Db	1	667	674	THPHFVRC	0.94	H-2-Kb
1	284	291	YHIFYQIL	0.26	H-2-Kb	1	1544	1553	SALEEAEASL	0.56	H-2-Db	1	260	268	ASADIETYL	0.94	H-2-Kb
1	764	772	KVFFKAGLL	0.26	H-2-Kb	1	311	321	YAFVSQGEVSV	0.57	H-2-Db	1	644	651	SSFQTVSA	0.95	H-2-Kb
1	420	428	QVYYSIGAL	0.26	H-2-Kb	1	487	495	QQFFNHHMF	0.57	H-2-Kb	1	1679	1687	RNNLLQAEL	0.95	H-2-Kb
1	834	841	LYFKIKPL	0.29	H-2-Kb	1	251	259	IHFGATGKL	0.57	H-2-Kb	1	267	275	YLLEKSRVI	0.96	H-2-Db
1	355	363	GAIMHYGNM	0.29	H-2-Kb	1	816	824	IQWNIRAFM	0.59	H-2-Kb	1	283	290	NYHIFYQI	0.96	H-2-Kb
1	76	84	VMQQNPPKF	0.3	H-2-Db	1	488	496	QFFNHHMFV	0.59	H-2-Kb	1	468	477	IFDFNSFEQL	0.97	H-2-Kb
1	487	494	QQFFNHHM	0.3	H-2-Kb	1	999	1009	KALQEAHQQAL	0.6	H-2-Db	1	1551	1561	ASLEHEEGKIL	0.98	H-2-Db
1	125	133	VNPYKWLPV	0.3	H-2-Kb	1	816	824	IQWNIRAFM	0.6	H-2-Db	1	1301	1308	SQLTRGKL	0.98	H-2-Kb
1	1291	1299	RQLEEKEAL	0.31	H-2-Db	1	1109	1117	KLKENQARI	0.6	H-2-Db	1	1102	1110	LALQLQKKL	0.99	H-2-Db
1	657	664	LNKLMTNL	0.31	H-2-Kb	1	709	716	KGFPNRIL	0.6	H-2-Kb	1	667	675	THPHFVRCI	0.99	H-2-Kb
1	320	330	SVASIDDSEEL	0.32	H-2-Db	1	1446	1454	KKQRNFDKI	0.61	H-2-Db						

Extended Data Table 3 | HLA types of healthy donors and patients with ICI-MC

Subject Identifier	HLA-A Condensed/Putative Allele Result	HLA-B Condensed/Putative Allele Result	HLA-C Condensed/Putative Allele Result	HLA-DPB1 Condensed/Putative Allele Result	HLA-DQA1 Condensed/Putative Allele Result	HLA-DQB1 Condensed/Putative Allele Result	HLA-DRB1 Condensed/Putative Allele Result	HLA-DRB3 Condensed/Putative Allele Result	HLA-DRB4 Condensed/Putative Allele Result	HLA-DRB5 Condensed/Putative Allele Result
Myocarditis Pt 1	03:01:01G + 24:02:01G	07:02:01G + 51:01:01G	01:02:01G + 07:02:01G	02:02:01G + 04:01:01G	01:02:01G + 05:01:01G	03:01:01i + 06:02:01i	11:01:01i + 15:01:01i	02:02:01i + NP	NP + NP	01:01:01i + NP
Myocarditis Pt 2	02:01:01G + 24:02:01G	39:06:02G + 40:02:01G	07:02:01G + 15:02:01G	03:01:01G + 06:01:01G	03:01:01G + 04:01:01G	03:01:01i + 04:02:01i	04:01:01i + 08:01:01i	NP + NP	01:01:01i + NP	NP + NP
Myocarditis Pt 3	01:01:01G + 03:01:01G	07:02:01G + 08:01:01G	07:01:01G + 07:02:01G	03:01:01G + 04:01:01G	01:02:01G + 05:01:01G	02:01:01i + 06:02:01i	03:01:01i + 15:01:01i	01:01:02i + NP	NP + NP	01:01:01i + NP
Healthy Donor 1	03:01:01G + 23:01:01G	07:02:01G + 44:03:01G	04:01:01G + 07:02:01G	02:01:02G + 02:01:02G	01:02:01G + 02:01:01G	02:02:01i + 06:02:01i	07:01:01i + 15:01:01i	NP + NP	01:01:01i + NP	01:01:01i + NP
Healthy Donor 2	02:06:01G + 30:01:01G	14:02:01G + 48:01:01G	08:02:01G + 08:03:01G	02:01:02G + 04:01:01G	01:01:01G + 03:01:01G	03:04:01i + 05:01:01i	01:02:01i + 04:03:01i	NP + NP	01:01:01i + NP	NP + NP
Healthy Donor 3	03:01:01G + 66:01:01G	41:02:01G + 57:01:01G	06:02:01G + 17:01:01G	04:01:01G + 04:01:01G	01:02:01G + 05:01:01G	03:01:01i + 05:02:01i	13:03:01i + 16:01:01i	01:01:02i + NP	NP + NP	02:02:01i + NP

nature portfolio

Corresponding author(s): Javid J. Moslehi and Justin M. Balko

Last updated by author(s): 9/22/2022

Reporting Summary

Nature Portfolio wishes to improve the reproducibility of the work that we publish. This form provides structure for consistency and transparency in reporting. For further information on Nature Portfolio policies, see our Editorial Policies and the Editorial Policy Checklist.

Statistics

For all statistical analyses, confirm that the following items are present in the figure legend, table legend, main text, or Methods section.

n/a	Confirmed
☐	☒ The exact sample size (*n*) for each experimental group/condition, given as a discrete number and unit of measurement
☐	☒ A statement on whether measurements were taken from distinct samples or whether the same sample was measured repeatedly
☐	☒ The statistical test(s) used AND whether they are one- or two-sided *Only common tests should be described solely by name; describe more complex techniques in the Methods section.*
☐	☒ A description of all covariates tested
☐	☒ A description of any assumptions or corrections, such as tests of normality and adjustment for multiple comparisons
☐	☒ A full description of the statistical parameters including central tendency (e.g. means) or other basic estimates (e.g. regression coefficient) AND variation (e.g. standard deviation) or associated estimates of uncertainty (e.g. confidence intervals)
☐	☒ For null hypothesis testing, the test statistic (e.g. *F*, *t*, *r*) with confidence intervals, effect sizes, degrees of freedom and *P* value noted *Give P values as exact values whenever suitable.*
☒	☐ For Bayesian analysis, information on the choice of priors and Markov chain Monte Carlo settings
☒	☐ For hierarchical and complex designs, identification of the appropriate level for tests and full reporting of outcomes
☒	☐ Estimates of effect sizes (e.g. Cohen's *d*, Pearson's *r*), indicating how they were calculated

Our web collection on statistics for biologists contains articles on many of the points above.

Software and code

Policy information about availability of computer code

Data collection	Flow cytometry data was collected with the Attune NxT Software v3.2.1. Light microscopy was performed with Olympus cellSens Standard imagine software version 1.17.
Data analysis	Flow cytometry data were analyzed using flowJo version 10.6. All other data were analyzed using R version 4.1.1 and R studio version 1.4.1106. Key R packages used include Seurat, vegan, and immunarch.

For manuscripts utilizing custom algorithms or software that are central to the research but not yet described in published literature, software must be made available to editors and reviewers. We strongly encourage code deposition in a community repository (e.g. GitHub). See the Nature Portfolio guidelines for submitting code & software for further information.

Data

Policy information about availability of data

All manuscripts must include a data availability statement. This statement should provide the following information, where applicable:

- Accession codes, unique identifiers, or web links for publicly available datasets
- A description of any restrictions on data availability
- For clinical datasets or third party data, please ensure that the statement adheres to our policy

Sequencing data have been deposited in the Gene Expression Omnibus (GEO) under accession number GSE213486. Source data are provided for all studies involving animals. An additional melanoma gene expression dataset was generated by the TCGA Research Network: https://www.cancer.gov/tcga and accessed using cBioPortal.

Field-specific reporting

Please select the one below that is the best fit for your research. If you are not sure, read the appropriate sections before making your selection.

☒ Life sciences ☐ Behavioural & social sciences ☐ Ecological, evolutionary & environmental sciences

For a reference copy of the document with all sections, see nature.com/documents/nr-reporting-summary-flat.pdf

Life sciences study design

All studies must disclose on these points even when the disclosure is negative.

Sample size	Sample size calculations were done with an alpha of 0.05 for 80% power where appropriate.
Data exclusions	Cells were excluded from single cell RNA sequencing analyses if they had less than 200 or more than 3000 unique transcripts or if greater than 15% of transcripts were of mitochondrial origin. Otherwise, no data were excluded.
Replication	All experiments were repeated for three biological replicates. All replicates yielded similar results.
Randomization	Mice were randomly assigned to treatment groups. Randomization is not relevant to other experiments presented. Relevant variables for interpreting each study are presented with the data.
Blinding	Experimenters were not blinded in these studies due to the low likelihood for bias in the particular experiments. For murine studies, since myocarditis produces physical symptoms, including death, and only mice of the Pdcd1 -/- Ctla4 +/- genotype present with these symptoms, blinding could not be successfully performed. For in vitro studies, knowledge of the individual sample is required for appropriate control of experimental variables (for ex. T cell receptor sequence/line and cognate antigen to be added to the same experimental sample); therefore there is no feasible way to blind investigators to these variables. Typically, blinding is done in 2 cases in the laboratory setting; biomarker studies and clinical interventional trials.

Reporting for specific materials, systems and methods

We require information from authors about some types of materials, experimental systems and methods used in many studies. Here, indicate whether each material, system or method listed is relevant to your study. If you are not sure if a list item applies to your research, read the appropriate section before selecting a response.

Materials & experimental systems

n/a	Involved in the study
☐	☒ Antibodies
☐	☒ Eukaryotic cell lines
☒	☐ Palaeontology and archaeology
☐	☒ Animals and other organisms
☐	☒ Human research participants
☒	☐ Clinical data
☒	☐ Dual use research of concern

Methods

n/a	Involved in the study
☒	☐ ChIP-seq
☐	☒ Flow cytometry
☒	☐ MRI-based neuroimaging

Antibodies

Antibodies used	anti-mouse CD45 (BioLegend; Alex Flour 488 cat# 103122; PerCP/Cy5.5 cat# 103132; clone 30-F11); anti-mouse CD3 (BioLegend, AF488 cat# 100210, clone 17A2), anti-mouse CD4 (BioLegend, APC cat# 100412, clone GK1.5), anti-mouse CD8a (BioLegend, PE/Cy7 cat# 100722, clone 53-6.7), anti-mouse/rat Thy1.1 (BioLegend, AF488 cat# 202506, Clone OX-7), anti-mouse TCR-beta chain (BioLegend, PE cat# 109208, Clone H57-597), anti-human CD3 (BioLegend, AF488 cat# 300319, clone HIT3a), anti-mouse CD4 (BioXCell, Cat# BE0003-1, clone GK1.5), anti-mouse CD8a (BioXCell, Cat# BE0061, clone 2.43), anti-mouse CD3 (Abcam, Ab16669, clone SP7), anti-mouse CD4 (eBioscience, 14–9766–82, clone 4SM95), anti-mouse CD8 (eBioscience, 14–0808–82, clone 4SM15), anti-mouse F4/80 (Novus Biologicals, NB600–404, clone CI-A3-1), anti-CD45R/B220 (cat# 553086, BD Pharmingen, clone RA3-6B2), anti-mouse IgG (Cat# BA-9200, Vector Laboratories, Inc., Burlingame, CA), anti-CD3-APC (BioLegend, cat# 100235, clone 17A2) and anti-CD8a-FITC (Thermo Fisher, cat # MA5-16759, clone KT15)
Validation	anti-mouse CD45 (BioLegend; Alex Flour 488 cat# 103122; PerCP/Cy5.5 cat# 103132; clone 30-F11) was validated by positive staining on mouse C57BL/6 splenocytes by flow cytometry. anti-mouse CD3 (BioLegend, AF488 cat# 100210, clone 17A2) was validated by positive staining on mouse C57BL/6 splenocytes by flow cytometry. anti-mouse CD4 (BioLegend, APC cat# 100412, clone GK1.5) was validated by positive staining on mouse C57BL/6 splenocytes relative to rat IgG2b, κ APC isotype control by flow cytometry. anti-mouse CD8a (BioLegend, PE/Cy7 cat# 100722, clone 53-6.7) was validated by positive staining on mouse C57BL/6 splenocytes. CD8a+ events were also positive for CD3 staining by flow cytometry.

anti-mouse/rat Thy1.1 (BioLegend, AF488 cat# 202506, Clone OX-7) was validated by positive staining on rat thymocytes by flow cytometry.
anti-mouse TCR-beta chain (BioLegend, PE cat# 109208, Clone H57-597) was validated by positive staining on mouse CD3+ C57BL/6 splenocytes by flow cytometry. TCR beta positive events were negative for staining with TCRγ/δ (UC7-13D5).
anti-human CD3 (BioLegend, AF488 cat# 300319, clone HIT3a) was validated by positive staining on Human peripheral blood lymphocytes by flow cytometry.
anti-mouse CD4 (BioXCell, Cat# BE0003-1, clone GK1.5) was validated by western blotting for purified mouse CD4 with C-terminal histidine tag.
anti-mouse CD8a (BioXCell, Cat# BE0061, clone 2.43) was validated by western blotting for purified mouse CD8a with C-terminal histidine tag.
anti-mouse CD3 (Abcam, Ab16669, clone SP7) was validated by western blotting for human, mouse, and rat thymus tissue lysate and IHC on rat spleen tissue, human tonsil tissue, and mouse epidydimal fat pad and lymph node tissues.
anti-mouse CD4 (eBioscience, 14–9766–82, clone 4SM95) was validated by IHC of formalin-fixed paraffin embedded mouse spleen.
anti-mouse CD8 (eBioscience, 14–0808–82, clone 4SM15) was validated by IHC of formalin-fixed paraffin embedded mouse spleen.
anti-mouse F4/80 (Novus Biologicals, NB600–404, clone CI-A3-1) was validated by IHC of formalin-fixed paraffin embedded mouse spleen.
anti-CD45R/B220 (cat# 553086, BD Pharmingen, clone RA3-6B2) was validated by flow cytometry on mouse splenocytes.
anti-mouse IgG (Cat# BA-9200, Vector Laboratories, Inc., Burlingame, CA) was validated for IHC.
anti-CD3-APC (BioLegend, cat# 100235, clone 17A2) was validated by positive staining on mouse C57BL/6 splenocytes by flow cytometry.
anti-CD8a-FITC (Thermo Fisher, cat # MA5-16759, clone KT15) was validated by positive staining on mouse splenocytes by flow cytometry.

Eukaryotic cell lines

Policy information about cell lines

Cell line source(s)	EL-4 cells were a gift from Dr. Simon Mallal and were originally obtained from the ATCC. Jurkat-TCR-ko-CD8+-NFAT-GFP reporter cells were a gift from Dr. Peter Steinberger. Unmodified Jurkat cells were originally obtained by ATCC.
Authentication	Jurkat-NFAT-GFP cells were validated by positive reporter activity by flow cytometry following overnight stimulation with PMA/ionomycin. Jurkat cell lines also were negative for TCR-beta chain and positive for CD8 by flow cytometry. EL-4 cells were validated by positive staining for mouse MHC-I by flow cytometry. All cells were also verified by morphology.
Mycoplasma contamination	All cells were negative for mycoplasma
Commonly misidentified lines (See ICLAC register)	None

Animals and other organisms

Policy information about studies involving animals; ARRIVE guidelines recommended for reporting animal research

Laboratory animals	Pdcd1-/-Ctla4+/-¬ mice were maintained as previously described (Wei, Meijers, et al, Cancer Discovery. 2021). Female mice were used in these studies due to their higher incidence of myocarditis. Rag1-/- mice were purchased from The Jackson Laboratory (#002216). C57BL/6J mice were purchased from The Jackson Laboratory (#000664). For the generation of survival curves, events were defined as either death (i.e., mice found dead) or identification of mice requiring euthanasia (e.g., due to lethargy, moribund, dyspnea, weight loss). All mice were housed at Vanderbilt University Medical Center vivarium, an Association for Assessment and Accreditation of Laboratory Animal Care International (AAALAC)–accredited, specific pathogen-free (SPF) animal facility. A mix of male and female mice were used. Sex is noted in each experiment. All mice were between 2-6weeks of age and age is noted for each experiment. Mice were on 12-h light–dark cycles which coincided with daylight in Nashville, TN. The mouse housing facility was maintained at 20–25 °C and 30–70% humidity
Wild animals	No wild animals were used in this study.
Field-collected samples	No field-collected samples were used in this study.
Ethics oversight	All experiments were performed in accordance with Vanderbilt University Medical Center Institutional Animal Care and Use Committee (IACUC) guidelines.

Note that full information on the approval of the study protocol must also be provided in the manuscript.

Human research participants

Policy information about studies involving human research participants

Population characteristics	Information for myocarditis patients is shown in Table 2. Healthy donors were 25-45 years of age, two were male and one was female.
Recruitment	All participants or families provided informed consent. Myocarditis patients were seen at VUMC and were recruited during their clinical care. There is not likely to be any relevant selection bias. Patients were recruited actively when notified by our clinical service that a patient had an immune related adverse event, and specifically for this study, myocarditis. Patients, or their families, were informed about the study and recruited if they were agreeable. Human healthy blood donors were recruited from around the medical campus by word of mouth.

Ethics oversight	All studies were conducted in accordance with the Declaration of Helsinki principles under protocols approved by the Vanderbilt University Medical Center (VUMC) Institutional Review Board. Healthy donors provided informed consent under an institutionally approved protocol (IRB# 030062). Myocarditis patients and families provided informed consent for research use of biospecimens and clinical data (IRB# 191213). ICI-colitis and Crohn's patients provided informed consent for research use of biospecimens and clinical data (IRB# 09109). Cardiac transplant and heart failure patients provide informed consent for research use of biospecimens and clinical data (IRB #200551).

Note that full information on the approval of the study protocol must also be provided in the manuscript.

Flow Cytometry

Plots

Confirm that:

☒ The axis labels state the marker and fluorochrome used (e.g. CD4-FITC).

☒ The axis scales are clearly visible. Include numbers along axes only for bottom left plot of group (a 'group' is an analysis of identical markers).

☒ All plots are contour plots with outliers or pseudocolor plots.

☒ A numerical value for number of cells or percentage (with statistics) is provided.

Methodology

Sample preparation	Single-cell suspensions were obtained from murine hearts by mincing followed by enzymatic digestion with 125 U/mL DNase I (Worthington; cat no. LS002138) and 250 U/mL Collagenase 3 (Worthington; cat no. LS004182). Dissociated hearts were filtered through a 30µm filter. Red blood cells were lysed using ACK lysing buffer (KD Medical/MediaTech; cat no. NC0274127). Single-cell suspensions were either used fresh or cryopreserved in 10% DMSO 90% FBS. Prior to sorting, cells were stained with Alex Flour 488 anti-mouse CD45 (BioLegend; clone 30-F11; cat no. 103122) for 20 minutes at 4°C. Following staining and washing with PBS, cells were resuspended in PBS with DAPI. Live CD45+ immune cells were sorted by fluorescence-activated cell sorting on AF488-positive DAPI-negative events. Expanded PBMCs (exPBMC) from patient 1 were prepared for single cell sequencing as follows. exPBMC were incubated with Human TruStain FcX™ (Fc Receptor Blocking Solution; BioLegend cat# 422302) for 5 minutes on ice, then washed and incubated with human anti-CD3-AF488 (BioLegend, cat# 300319, clone HIT3a) for 30 minutes on ice, and then washed and resuspended to a concentration of 5x105 cells/mL. SYTOX AADvanced™ Ready Flow™ Reagent (Invitrogen, cat# R37173) was used following the manufacturer's instructions to exclude dead cells. CD3+ live cells were sorted on the WOLF cell sorter (Nanocellect).
Instrument	Samples were run on an Attune NxT Acoustic Focusing Cytometer (Life Technologies).
Software	FlowJo version 10.6.
Cell population abundance	Cell purity was assessed following sorting in single cell RNA sequencing in extended data figures.
Gating strategy	Gating was first done on forward scatter and side scatter to exclude debris. Doublets were excluded by gating on FSC area versus FSC height. DAPI was used to exclude dead cells from analyses. For tetramer experiments, live cells were gated on CD3+CD8+ double positive cells.

☒ Tick this box to confirm that a figure exemplifying the gating strategy is provided in the Supplementary Information.